RESEARCH ARTICLE SUMMARY

NEUROIMMUNOLOGY

Reversible CD8 T cell–neuron cross-talk causes aging-dependent neuronal regenerative decline

Luming Zhou†, Guiping Kong†, Ilaria Palmisano, Maria Teresa Cencioni, Matt Danzi, Francesco De Virgiliis, Jessica S. Chadwick, Greg Crawford, Zicheng Yu, Fred De Winter, Vance Lemmon, John Bixby, Radhika Puttagunta, Joost Verhaagen, Constandina Pospori, Cristina Lo Celso, Jessica Strid, Marina Botto, Simone Di Giovanni*

INTRODUCTION: Axonal regeneration and neurological functional recovery are extremely limited in the elderly. Consequently, injuries to the nervous system are typically followed by severe and long-term disability. Our understanding of the molecular mechanisms underlying aging-dependent regenerative failure is poor, hindering progress in the development of effective therapies for neurological repair. To facilitate the design of repair strategies, there is a pressing need to identify critical molecular and cellular mechanisms that cause regenerative failure in aging.

RATIONALE: Aging causes a broad spectrum of modifications in cell signaling, including changes in metabolism, immunity, and overall tissue homeostasis, which play key roles in nervous system physiology and response to insults. Thus, we hypothesized that injuries to the aged nervous system would be followed by unique molecular and cellular modifications that would contribute to aging-dependent regenerative decline. To this end, molecular and cellular signatures associated with aging and injury to the nervous system were systematically investigated by performing RNA sequencing from dorsal root ganglia (DRG) in a well-established model of sciatic nerve injury in young versus aged mice. Insight into these mechanisms could allow the discovery of previously unrecognized molecular targets to counteract aging-dependent regenerative decline.

RESULTS: Initial analysis of RNA sequencing data identified that aging was mainly associated with a marked increase in T cell activation and signaling in DRG after sciatic nerve injury in mice. Subsequent experiments demonstrated that aging was associated with increased inflammatory cytokines including lymphotoxins in DRG both preceding and following sciatic nerve injury. Specifically, we found that lymphotoxin β was required for the phosphorylation of NF-κB that drives the expression of the chemokine CXCL13 in DRG sensory neurons. CXCL13 attracted $CD8^+$ T cells that expressed the CXCL13 receptor CXCR5 in proximity to neurons that act as antigen-presenting cells by overexpressing major histocompatibility complex class I (MHC I) after a sciatic nerve injury. The engagement of $CXCR5^+CD8^+$ T cells with MHC I–expressing sensory neurons activated caspase 3, which impaired pAKT and pS6 signaling, leading to regenerative failure. Pharmacological antagonism of caspase 3 activation reversed regenerative failure in aged animals and restored pAKT and pS6 expression. Adoptive transfer experiments including comparison between *Cxcr5*$^{-/-}$ and wild-type cells directly implicated $CXCR5^+CD8^+$ T cells in restricting axonal regeneration after sciatic injury in the aged animals. Finally, neutralization of CXCL13 with monoclonal antibodies antagonized the recruitment of $CXCR5^+CD8^+$ T cells to the DRG and restored the regenerative ability of sciatic sensory axons in aged mice to levels comparable to those found in young animals. CXCL13 antagonism also significantly promoted skin reinnervation and neurological recovery of sensory function.

CONCLUSION: We have identified an aging-dependent mechanism that relies on the CXCL13-dependent recruitment and activation of $CXCR5^+CD8^+$ T cells in proximity to sensory neurons that restrict axonal regeneration after nerve injury after communication with MHC I–presenting DRG neurons. CXCL13 antagonism with humanized monoclonal antibodies can revert regenerative decline and promote neurological recovery in aged mice, suggesting a pathway that could be exploited in future therapies. ■

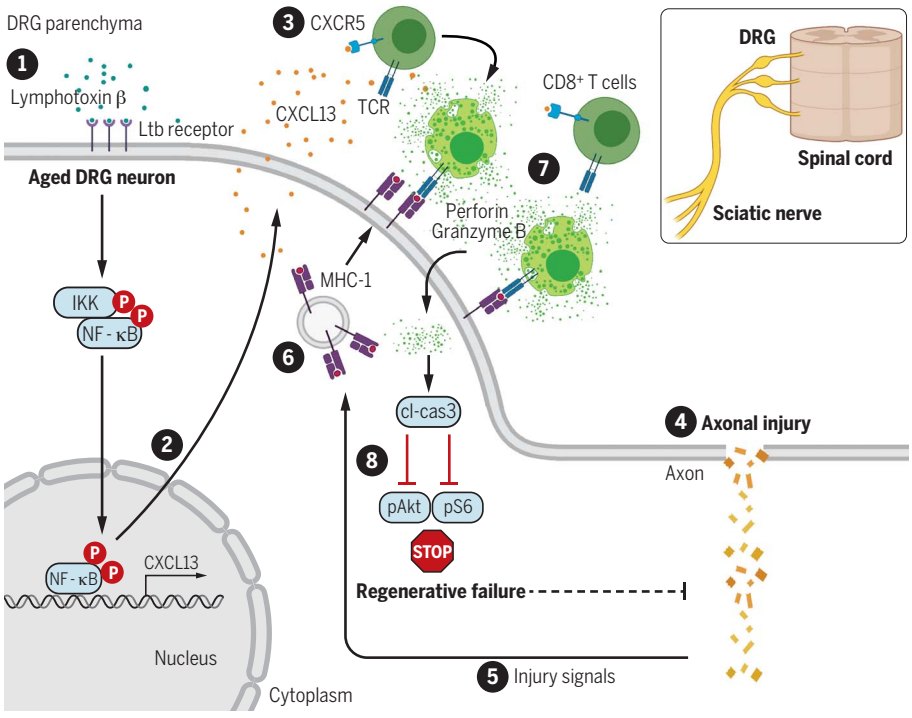

Sequence of events leading to aging-dependent regenerative failure in injured sensory neurons. (1) Lymphotoxin β activates NF-κB; (2) phosphorylated NF-κB increases CXCL13 expression; (3) $CXCR5^+CD8^+$ T cells are recruited into the DRG parenchyma; (4 and 5) sciatic axonal injury activates injury signals; (6) MHC I is presented by DRG neurons; (7) $CXCR5^+CD8^+$ T cells engage with MHC I and activate neuronal caspase 3; (8) cleaved caspase 3 reduces pAKT and pS6, leading to regenerative failure.

The list of author affiliations is available in the full article online.
*Corresponding author. Email: s.di-giovanni@imperial.ac.uk
†These authors contributed equally to this work.
Cite this article as L. Zhou *et al.*, *Science* **376**, eabd5926 (2022). DOI: 10.1126/science.abd5926

READ THE FULL ARTICLE AT
https://doi.org/10.1126/science.abd5926

RESEARCH ARTICLE

NEUROIMMUNOLOGY

Reversible CD8 T cell–neuron cross-talk causes aging-dependent neuronal regenerative decline

Luming Zhou[1]†, Guiping Kong[1]†, Ilaria Palmisano[1], Maria Teresa Cencioni[2], Matt Danzi[3], Francesco De Virgiliis[1], Jessica S. Chadwick[1], Greg Crawford[4], Zicheng Yu[1], Fred De Winter[5], Vance Lemmon[3], John Bixby[3], Radhika Puttagunta[6], Joost Verhaagen[5], Constandina Pospori[7,8], Cristina Lo Celso[7,8], Jessica Strid[4], Marina Botto[4], Simone Di Giovanni[1]*

Aging is associated with increased prevalence of axonal injuries characterized by poor regeneration and disability. However, the underlying mechanisms remain unclear. In our experiments, RNA sequencing of sciatic dorsal root ganglia (DRG) revealed significant aging-dependent enrichment in T cell signaling both before and after sciatic nerve injury (SNI) in mice. Lymphotoxin activated the transcription factor NF-κB, which induced expression of the chemokine CXCL13 by neurons. This in turn recruited CXCR5$^+$CD8$^+$ T cells to injured DRG neurons overexpressing major histocompatibility complex class I. CD8$^+$ T cells repressed the axonal regeneration of DRG neurons via caspase 3 activation. CXCL13 neutralization prevented CXCR5$^+$CD8$^+$ T cell recruitment to the DRG and reversed aging-dependent regenerative decline, thereby promoting neurological recovery after SNI. Thus, axonal regeneration can be facilitated by antagonizing cross-talk between immune cells and neurons.

With aging, there is a decline in axonal regenerative ability that undermines recovery and often leads to long-term disability (*1*–*4*). The cellular and molecular mechanisms underlying aging-dependent regenerative decline remain poorly understood. Previous studies have shown that an age-related impairment in dedifferentiation and activation of Schwann cells limits axonal regrowth in the injured peripheral nervous system, impairing sensory and motor recovery (*5*, *6*).

Aging itself produces a wide range of profound modifications in cell signaling, metabolism, immunity, gene regulation, and protein translation, which affect tissue homeostasis (*7*–*9*). Therefore, we hypothesized that aging involves the development of unique molecular and cellular mechanisms preceding injury, which, in combination with injury-specific signals, would prime neurons toward regenerative failure. A better understanding of these mechanisms could allow the identification of additional molecular strategies to counteract aging-dependent regenerative decline.

[1]Division of Neuroscience, Department of Brain Sciences, Imperial College London, London, UK. [2]Division of Neurology, Department of Brain Sciences, Imperial College London, London, UK. [3]Miami Project to Cure Paralysis, Department of Neurological Surgery, Miller School of Medicine, University of Miami, Miami, FL, USA. [4]Department of Immunology and Inflammation, Imperial College London, London, UK. [5]Netherlands Institute for Neuroscience, Royal Academy of Arts and Sciences, Amsterdam, Netherlands. [6]Spinal Cord Injury Center, Heidelberg University Hospital, Heidelberg, Germany. [7]Haematopoietic Stem Cell Laboratory, Francis Crick Institute, London, UK. [8]Department of Life Sciences, Imperial College London, South Kensington Campus, London, UK.
*Corresponding author. Email: s.di-giovanni@imperial.ac.uk
†These authors contributed equally to this work.

RNA sequencing (RNA-seq) of sciatic nerve dorsal root ganglia (DRG) in mice identified an aging-dependent enrichment in immune and cytokine/chemokine signaling that intensified after sciatic nerve injury. The aging-dependent increase in inflammatory cytokines, including lymphotoxin, activated NF-κB in DRG neurons, which up-regulated expression of the chemokine CXCL13. CXCL13 in turn recruited CXCR5$^+$CD8$^+$ T cells to sites near neurons acting as antigen-presenting cells (APCs) by overexpressing major histocompatibility complex class I (MHC I). Activated CD8$^+$ T cells repressed axonal regeneration of sensory DRG neurons by inhibiting regenerative signals via caspase 3–dependent reduction in pAKT and pS6. In vivo CD8$^+$ T cell depletion or CXCL13 neutralization restored axonal regeneration of sensory neurons promoting functional recovery.

Thus, we identify an aging-dependent mechanism restricting the regenerative ability of axons. Moreover, we propose antibody-mediated manipulation of neuron–immune cell cross-talk as a clinically suitable approach for neurological repair in the elderly.

Aging induces extensive changes in adaptive immune gene profiles in sciatic DRG at homeostasis and after injury

RNA-seq was performed on sciatic DRG from 8- to 10-week-old (young) versus 20- to 22-month-old (aged) mice either preceding (sham) or following a sciatic nerve injury (SNI). Changes in gene expression were compared to the baseline expression in young sham animals. Significantly differentially expressed genes [false discovery rate (FDR) < 0.05] were analyzed by Gene Ontology (GO) and Kyoto Encyclopedia of Genes and Genomes (KEGG) for functional classification (Fig. 1A, fig. S1A, and data S1 and S2). The highest number of significantly differentially expressed genes (FDR < 0.05) was identified in aged DRG after injury (fig. S1, B to D, and data S1). The down-regulation of GO classes implicated in neurodevelopment, neurotransmitters, ion transport, G protein–coupled signaling, and signal transduction observed in young animals failed to occur in aged DRG even after SNI (Fig. 1A and data S2). Aged DRG displayed a marked enrichment in gene expression associated with adaptive immune responses, especially T cell and cytokine/chemokine signaling, which was amplified after SNI (Fig. 1A, fig. S1A, and data S2). The prominent aging-dependent regulation of the immune response was then prioritized for further analysis. A shortlist of 310 transcripts (data S3) enriched for immune response according to GO and KEGG ($P < 0.01$) was used to map hypothetical signaling networks. The network revealed interconnected functional clusters including chemokine-cytokine interactions and B and T cell signaling (Fig. 1B). Notably, the aging-dependent T cell responses coincided with a major increase in the number of T cell receptor (TCR) clonotypes (fig. S1E).

Neuronal CXCL13 is elevated in aged DRG along with CD8$^+$ T cells expressing CXCR5

Cxcl13 was the most prominently up-regulated gene after sciatic injury (Fig. 1C and data S3). The expression of the CXCL13 receptor *Cxcr5* was also significantly enhanced in aged DRG (Fig. 1C and data S3), suggesting the presence of a CXCL13-CXCR5 signaling axis. A significant increase in CXCL13 expression was also observed in aged sciatic DRG neurons both at baseline and 3 days after SNI, when regeneration is reduced relative to young DRG neurons (Fig. 1, D to H, and fig. S1, F to H). Although Cxcl13 expression was also detected around the sciatic nerve injury site, no aging-dependent changes were observed (fig. S1, I and J). CXCL13 protein in DRG 3 days after SNI also significantly increased in the aged DRG group relative to young DRG mice (Fig. 1I).

Because CXCL13 is a chemoattractant for CXCR5$^+$ B and T cells, we next assessed the localization and immunophenotype of B and T cells within the DRG 3 days after SNI in young or aged mice. B and T cells including CXCR5$^+$ B cells, CXCR5$^+$CD8$^+$ T cells, and CD4$^+$ T cells significantly increased in aged DRG parenchyma (Fig. 2, A to D, and fig. S2, A to F).

A considerable percentage of CXCR5$^+$CD8$^+$ T cells were CD44$^+$CD69$^+$CD62L$^-$, indicating effector memory T cells (Fig. 2, E and F, and fig. S2D), whereas only a very small proportion of CD8$^+$ T cells or CXCR5$^+$CD8$^+$ T cells were CD103$^+$ and P2RX7$^+$, suggesting a migratory rather than a primary tissue-resident phenotype. Approximately half of both CD8$^+$ and

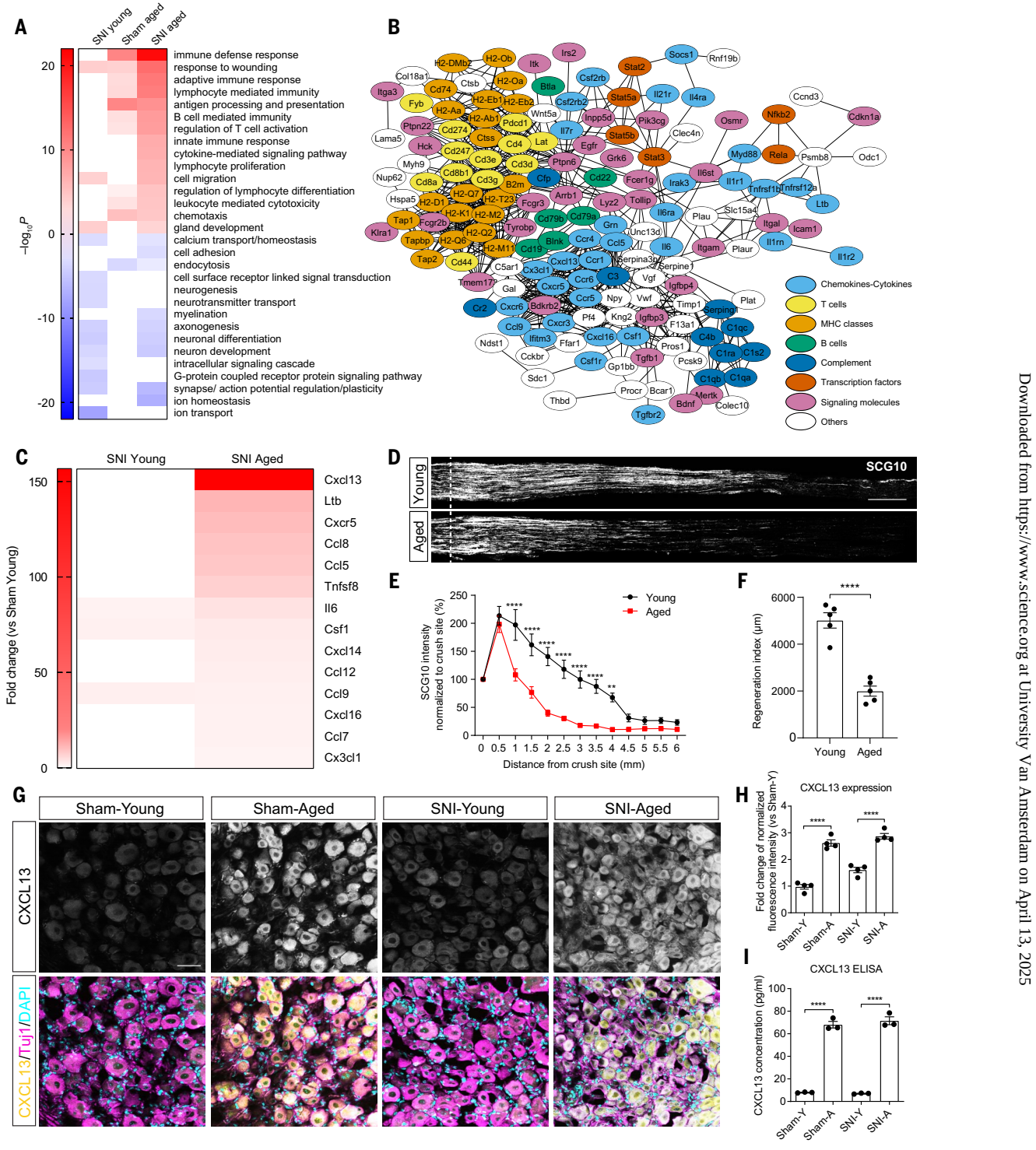

Fig. 1. Aging induces enrichment in genes associated with chemokine and cytokine expression and adaptive immunity in dorsal root ganglia, including after SNI. (**A**) Heatmap shows the top 15 categories of Gene Ontology Biological Processes (GO-BPs) of the differentially expressed genes (FDR < 0.05) from three comparisons: SNI young, sham aged, and SNI aged versus sham young, respectively (n = 3). GO-BPs enrichment of up-regulated (red) and down-regulated (blue) are indicated by $-\log_{10}P$ (P < 0.01). (**B**) Cytoscape visualization of the STRING protein-protein interaction network of the up-regulated genes (FDR < 0.05) involved in immune response in SNI aged versus sham young (P < 0.01). Each node is a gene, color-coded according to STRING functional annotation. (**C**) Heatmap shows the fold change of the differentially expressed chemokines and cytokines. (**D**) Representative SCG10 immunostaining of sciatic nerves 3 days after SNI. The dashed line indicates the proximal crush site. Scale bar, 500 μm. (**E**) Normalized SCG10 intensity to the proximal crush site (n = 5). (**F**) Analysis of the regeneration index (n = 5). (**G**) Representative immunostaining of CXCL13, the neuronal marker Tuj1, and DAPI in DRG 3 days after SNI. Scale bar, 50 μm. (**H**) Quantification of CXCL13 expression shown in (G) (n = 4). (**I**) CXCL13 ELISA from sciatic DRG (n = 3). **P < 0.01, ****P < 0.0001 [two-way ANOVA with post hoc Sidak's test in (E); unpaired Student's t test in (F); one-way ANOVA with post hoc Tukey's test in (H) and (I)]. Data are means ± SEM and represent three [(A), (C), and (I)] or two [(E), (F), and (H)] experiments.

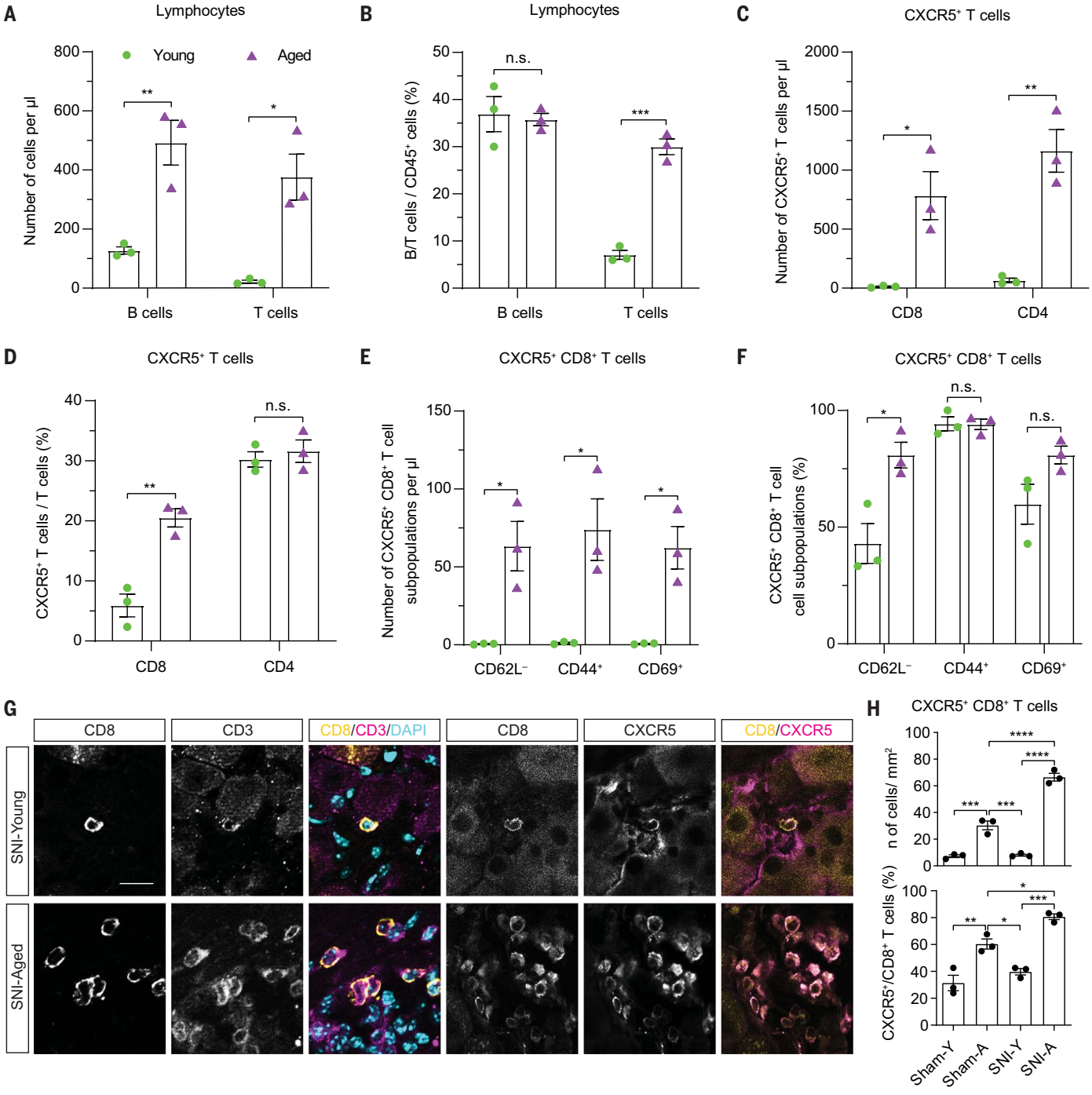

Fig. 2. CXCR5$^+$CD8$^+$ T cell characterization in DRG before and after SNI. (**A**) Quantification of B and T cell number normalized to the counting beads in DRG (n = 3). (**B**) Percentage of B and T cells of total CD45$^+$ cells in DRG (n = 3). (**C**) Number of CXCR5$^+$CD8$^+$ or CD4$^+$ T cells normalized to the counting beads in DRG (n = 3). (**D**) Percentage of CXCR5$^+$CD8$^+$ or CD4$^+$ T cells in DRG (n = 3). (**E**) Number of CD62L$^-$, CD44$^+$, or CD69$^+$/CXCR5$^+$CD8$^+$ T cells normalized to the counting beads in DRG (n = 3). (**F**) Percentage of CD62L$^-$, CD44$^+$, or CD69$^+$/CXCR5$^+$CD8$^+$ T cells in DRG (n = 3). (**G**) CD8 coimmunostained with CD3 and DAPI or CXCR5 in DRG 3 days after SNI. Scale bar, 10 µm. (**H**) Quantification of CXCR5$^+$CD8$^+$ T cell number and percentage of CXCR5$^+$CD8$^+$ T cells of total CD8$^+$ T cells in DRG in sham or 3 days after SNI (n = 3). *P < 0.05, **P < 0.01, ***P < 0.001, ****P < 0.0001 [unpaired Student's t test in (A) to (F) or one-way ANOVA with post hoc Tukey's test in (H)]; n.s., not significant. Data are means ± SEM and represent three experiments.

CXCR5$^+$CD8$^+$ T cells also expressed CXCR6, suggesting cell retention and restricted recirculation ability (fig. S3).

In aged animals, the percentage of naïve total T cells in the blood was reduced, whereas the percentage of memory CXCR5$^+$ T cells was significantly enhanced (fig. S4). The number of CD8$^+$ T cells, including CXCR5$^+$CD8$^+$ T cells, significantly increased in aged sciatic DRG relative to young at baseline, with a further significant increase 3 days after SNI (Fig. 2, G and H). All CD8$^+$ cells were CD68$^-$ and CD3$^+$, indicating that they were T cells and not macrophages (fig. S5A). Finally, B cell numbers in aged DRG after SNI increased, but these cells

localized outside of the DRG parenchyma, likely in the perivenular space (fig. S5, B and C). Thus, aging is associated with enhanced neuronal expression of CXCL13 and recruitment of CXCR5$^+$ active and resident T cells to the DRG parenchyma before and after SNI.

Neuronal CXCL13 is sufficient to recruit CXCR5$^+$ B and T cells to the DRG and to impair axonal regeneration

Next, we asked whether CXCL13 was secreted and whether its overexpression was sufficient to recruit CXCR5$^+$ B and T cells to the DRG. We first transduced cultured DRG neurons with adeno-associated virus (AAV) to overexpress CXCL13, and culture medium was collected for the subsequent in vitro splenocyte migration assays. Medium from CXCL13-overexpressing cultures versus control enhanced the recruitment of CXCR5$^+$ B and T cells (fig. S6).

To address whether CXCL13 expression would affect axonal regeneration, we overexpressed CXCL13 in vivo in DRG neurons, and interferon-γ (IFN-γ) and mannitol were delivered systemically to induce MHC I presentation and enhance blood-DRG barrier permeability, respectively. Immediately thereafter, a SNI was performed (fig. S7). Both CXCR5$^+$ B and CXCR5$^+$CD8$^+$ T cells were significantly increased in *Cxcl13*-overexpressing DRG relative to green fluorescent protein (GFP) control (Fig. 3, A to F). Sciatic nerve axonal regeneration was significantly reduced after *Cxcl13* overexpression (Fig. 3, G to I).

Thus, CXCL13 expressed by DRG neurons can recruit CXCR5$^+$ B and T cells and can inhibit axonal regeneration, partially phenocopying the aging phenotype.

CXCL13 expression in aged DRG requires lymphotoxin-dependent NF-κB phosphorylation

To identify the transcription factors (TFs) putatively involved in driving aging-dependent CXCL13 expression, we asked whether TFs previously reported to promote CXCL13 expression were induced in aged DRG in our RNA-seq dataset. Among the TFs known to bind to the CXCL13 promoter—including *Hif1a*,

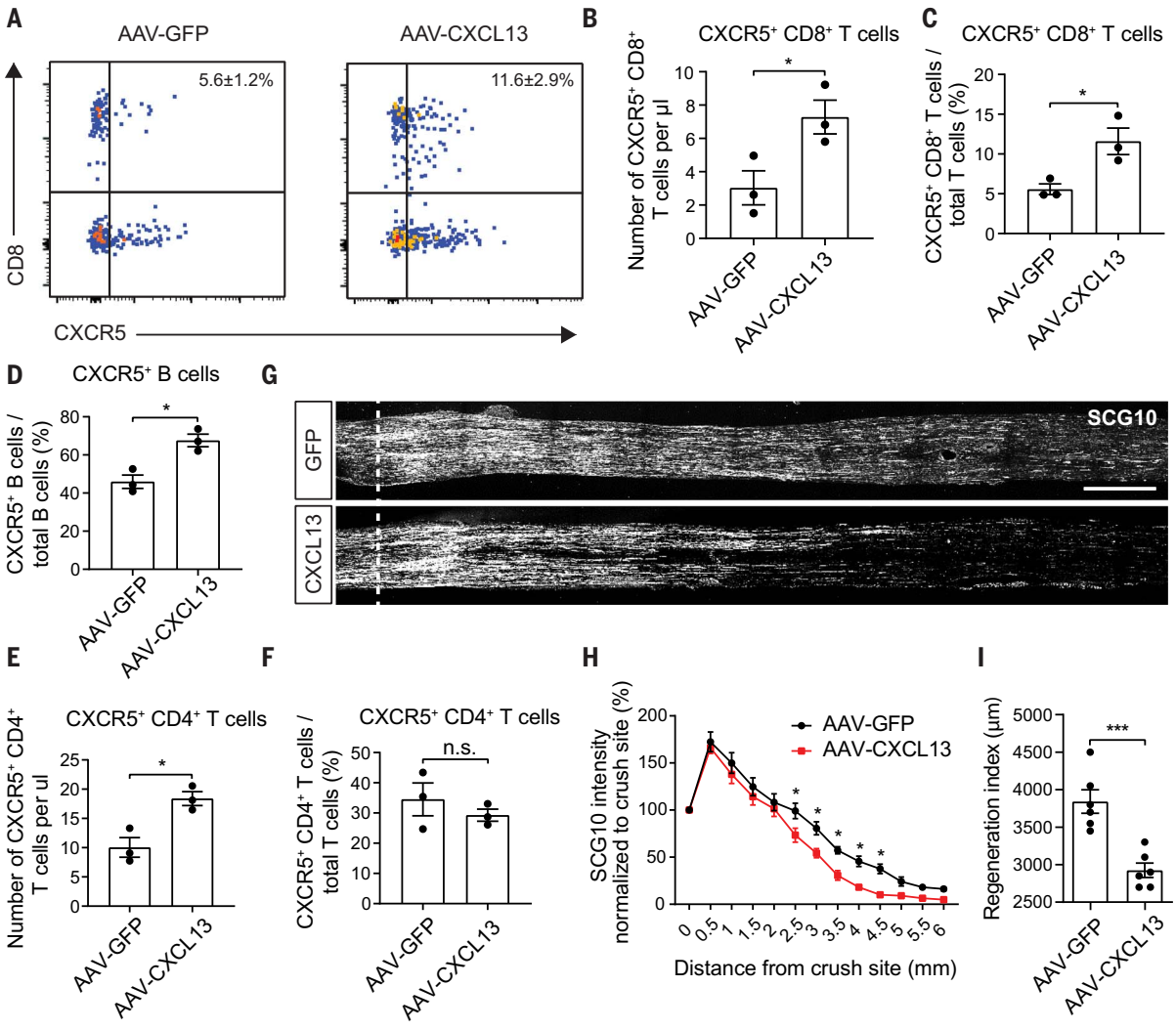

Fig. 3. Overexpression of CXCL13 in DRG neurons in young mice facilitates the recruitment of CXCR5$^+$ B and T cells to the DRG and reduces sciatic nerve regeneration. (**A**) Flow cytometry analysis of CXCR5$^+$CD8$^+$ T cells in AAV-GFP– or AAV-*Cxcl13*–infected sciatic DRG 3 days after SNI. (**B**) Quantification of CXCR5$^+$CD8$^+$ T cell number normalized to the counting beads in the sciatic DRG (n = 3). (**C**) Percentage of CXCR5$^+$CD8$^+$ T cells in sciatic DRG (n = 3). (**D**) Percentage of CXCR5$^+$ B cells in sciatic DRG (n = 3). (**E**) Number of CXCR5$^+$CD4$^+$ T cells in sciatic DRG normalized to the counting beads (n = 3). (**F**) Percentage of CXCR5$^+$CD4$^+$ T cells in sciatic DRG (n = 3). (**G**) Representative SCG10 immunostaining of sciatic nerves from AAV-GFP– or AAV-*Cxcl13*–infected mice. The dashed line indicates the proximal injury site. Scale bar, 500 µm. (**H**) Normalized SCG10 intensity to the proximal crush site from the mice infected with AAV-GFP and AAV-*Cxcl13* (n = 6). (**I**) Analysis of the regeneration index (n = 6). *P < 0.05, ***P < 0.001 [unpaired Student's t test in (B), (C), (D), (E), (F), and (I) or two-way ANOVA with post hoc Sidak's test in (H)]. Data are means ± SEM and represent three experiments.

Pou5f1 (*Oct4*), *Rar*, *Nfkb*, and *Sp1* (*10*, *11*)—only *Nfkb2* was significantly up-regulated in aged DRG, which made it a candidate for further investigation (fig. S8A). We next treated cultured DRG neurons with canonical NF-κB activators [tumor necrosis factor–α (TNF-α) or interleukin-1β (IL-1β)] and noncanonical NF-κB activators (BAFF or LTα1β2) for 24 hours, followed by reverse transcription polymerase chain reaction (RT-PCR) for *Cxcl13*, *Nfkb1*, and *Nfkb2*. TNF-α and IL-1β were able to up-regulate the expression of *Nfkb1* and/or *Nfkb2* but not *Cxcl13*, whereas BAFF affected neither *Nfkb* nor *Cxcl13* gene expression (fig. S8B).

However, LTα1β2, which is known to activate noncanonical NF-κB2 (*12*), significantly enhanced the expression of both *Nfkb2* and *Cxcl13*. This effect could be attenuated via the selective inhibition of the NF-κB kinase IKK using the IKK inhibitor PS1145 (fig. S8C). Both NF-κB2 expression and phosphorylation were induced with aging, but phosphorylation of NF-κB2 was inhibited by PS1145 relative to a vehicle control (fig. S8D). Accordingly, aging-induced expression of *Cxcl13* was significantly decreased by PS1145 (fig. S8E). Finally, immunostaining for pNF-κB2 demonstrated neuronal localization within the DRG and a significant increase in aged DRG neurons both before and 3 days after SNI (fig. S8, F and G). Thus, age-related expression of CXCL13 is driven by NF-κB2.

CD8$^+$ T cells and neuronal MHC I are required for aging-dependent regenerative decline after sciatic nerve injury

Next, we asked whether CD8$^+$ T cells, CD4$^+$ T cells, or B cells are required to impair axonal regeneration of aged sciatic DRG neurons. When CD8$^+$ T cells were depleted using a CD8α monoclonal antibody (mAb) administered to aged mice 1 week before SNI, we observed significantly improved nerve regeneration (Fig. 4, A to C) and a significant reduction of CD8$^+$ T cells in the DRG relative to animals that received an isotype control (fig. S9). By contrast, the depletion of CD4$^+$ T or B cells did not alter aging-dependent regenerative decline after SNI (fig. S10).

These data implicate CD8$^+$ T cells in the regenerative decline that follows SNI in aged animals. RNA-seq revealed an aging-dependent enrichment in the expression of MHC I after SNI (Fig. 1B). MHC I expression increased before and after SNI in aged DRG neurons relative to young controls (Fig. 4, D to F). MHC I expression did not show any selectivity for neuronal subtypes (fig. S11, A to C). However, MHC I was not expressed in axons, but rather was restricted to macrophages in proximity to the sciatic nerve lesion site (fig. S11D).

Next, we asked whether antigen-sensitized CD8$^+$ T cells were required to limit neurite outgrowth in MHC I–expressing DRG neurons in culture. MHC I was induced in DRG neurons but absent in glial cells after IFN-γ injection (fig. S12, A to D). TCR-transgenic OT-I CD8$^+$ T cells effected reduced neurite outgrowth in DRG neurons expressing MHC I in the presence of the ovalbumin (OVA) peptide $OVA_{257–264}$ (fig. S12, E and F) as well as an increase in cleaved caspase 3 without an increase in apoptotic features (fig. S12, G and H). The purity of isolated CD8$^+$ T cells from the spleen of OT-I mice was confirmed by flow cytometry (fig. S12I). Thus, the presence of both neuronal MHC I expression and OT-I antigen-specific CD8$^+$ T cells is needed to reduce neurite outgrowth in DRG neurons.

We next explored whether MHC I–dependent peptide presentation was needed for axonal regenerative decline in aging mice. To this end, we used AAV to conditionally express the virally encoded glycine/alanine-rich peptide sequence GAr, which inhibits MHC I antigen presentation, thereby evading CD8$^+$ T cell immune responses (*13*, *14*), in sciatic DRG of aged mice (fig. S13A). A sciatic nerve crush injury was then performed and animals were killed 3 days later (fig. S13B). Neuronal MHC I and cleaved caspase 3 expression were significantly reduced after AAV-GAr-rtTA infection relative to control AAV-rtTA (Fig. 4, G and H). Sciatic axonal regeneration was significantly enhanced upon AAV-GAr-rtTA infection (Fig. 4, I and J, and fig. S13, C to E). Thus, both CD8$^+$ T cells and neuronal MHC I are required for aging-dependent regenerative decline after SNI.

CD8$^+$ T cell–dependent activation of caspase 3 inhibits pAKT and pS6 and is required for aging-dependent axonal regenerative failure

We aimed to characterize the molecular signaling underpinning CD8$^+$ T cell–dependent regenerative decline in aged animals. Cleaved caspase 3 expression significantly increased in DRG neurons of aged mice 3 days after SNI (Fig. 4, K and L) in the absence of DNA fragmentation associated with apoptosis (fig. S14A). Perforin and granzyme B expression significantly increased in aged DRG neurons after SNI (fig. S14, B to D). Active caspase 3 can lead to AKT truncation and reduced AKT phosphorylation (*15*), which in turn reduces S6 phosphorylation. pAKT and pS6 are associated with axonal regeneration (*16*, *17*) and are typically impaired by aging (*18*). Indeed, phosphorylation of AKT and S6 decreased in aged DRG 3 days after SNI. However, this effect was significantly reversed after depletion of CD8$^+$ T cells (Fig. 4, M and N). CD8$^+$ T cell depletion significantly enhanced pAKT and pS6 in DRG neurons while reducing the expression of cleaved caspase 3, perforin, and granzyme B (fig. S14, E to G, and fig. S15, A and B).

Finally, the inhibition of caspase 3 with Z-DEVD-FMK significantly induced AKT and S6 phosphorylation (fig. S15, C and D) and increased sciatic axon regeneration (fig. S15, E to G). Thus, CD8$^+$ T cell–dependent activation of caspase 3 is required to inhibit pAKT and pS6 in aged DRG neurons after SNI. Moreover, the inhibition of caspase 3 activation promotes axonal regeneration.

CXCR5$^+$CD8$^+$ T cells drive aging-dependent axonal regenerative decline after sciatic nerve injury

Next, we sought to determine whether CXCR5$^+$ CD8$^+$ T cells are directly responsible for axonal regenerative decline after SNI. CXCR5$^+$CD8$^+$ T cells were isolated and adoptively transferred to young or aged OT-I *Rag2*$^{-/-}$ mice, which lack B and T cells (fig. S16A). Prior to cell transfer, we found a significant increase in nerve regeneration from aged OT-I *Rag2*$^{-/-}$ mice with and without CD8 T cell depletion relative to wild-type mice, with no change between the two OT-I *Rag2*$^{-/-}$ groups (fig. S16, B to E). Thus, endogenous OT-I CD8$^+$ T cells had no effect on nerve regeneration.

We then asked whether adoptive transfer of CXCR5$^+$CD8$^+$ T cells was sufficient to restrict sciatic nerve regeneration in aged mice after SNI. Sorted CXCR5$^+$CD8$^+$ T cells (fig. S17, A and B) were injected into young or aged OT-I *Rag2*$^{-/-}$ recipients. Adoptively transferred CXCR5$^+$CD8$^+$ T cells robustly infiltrated aged DRG, but not young recipients (Fig. 5, A and B). By contrast, transferred CXCR5$^+$CD8$^+$ T cells accumulated more abundantly in spleens of young mice versus aged mice (Fig. 5, A and B). These migratory patterns of CXCR5$^+$CD8$^+$ T cells correlated with the differential CXCL13 levels in the DRG and spleens (Fig. 5C). Additionally, transferred CXCR5$^+$CD8$^+$ T cells were increased in the blood of aged mice (fig. S17, C and D). Finally, adoptive transfer of CXCR5$^+$CD8$^+$ T cells led to a significantly reduced sciatic nerve regeneration after injury in aged mice alone (Fig. 5, D and E, and fig. S17E). CXCR5$^+$CD8$^+$ T cell transfer resulted in a significant increase of perforin and a decrease of pS6 expression in aged DRG neurons (Fig. 5, F and G), whereas no changes were noted in the DRG of young mice (fig. S17, F to I).

CXCL13 antagonism blocks the recruitment of CXCR5$^+$CD8$^+$ T cells to rescue aging-dependent axonal regenerative decline after sciatic nerve injury

Having demonstrated that recruitment of CXCR5$^+$CD8$^+$ T cells causes regeneration failure, we asked how these cells are recruited. Sorted wild-type or *Cxcr5*$^{-/-}$ CD8$^+$ T cells were transferred to OT-I *Rag2*$^{-/-}$ recipient mice that were treated with control immunoglobulin G (IgG) or CXCL13 mAb before SNI. *Cxcr5*$^{-/-}$ CD8$^+$ T cell recruitment to the DRG was significantly lower than for wild-type CD8$^+$ T cells. CXCL13 mAb significantly reduced the migration

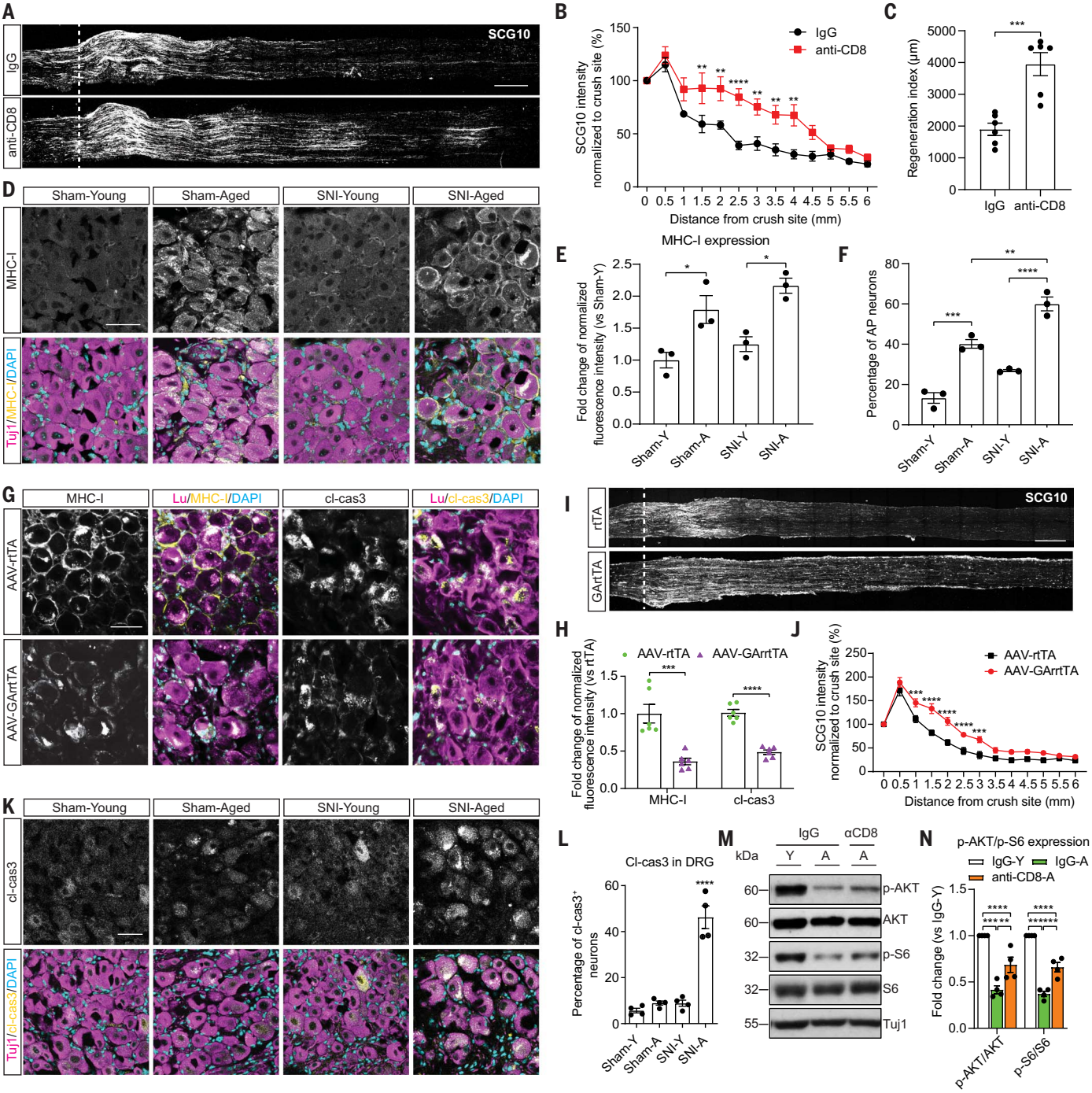

Fig. 4. CD8⁺ T cells and neuronal MHC I are required for age-dependent regenerative decline after SNI through pAKT and pS6. (**A**) Representative SCG10 immunostaining of sciatic nerves 3 days after SNI after control IgG or CD8 mAb. The dashed line indicates the proximal crush site. Scale bar, 500 μm. (**B**) Normalized SCG10 intensity to the proximal crush site (n = 6). (**C**) Analysis of regeneration index (n = 6). (**D**) Representative MHC I and Tuj1 coimmunostaining and DAPI in sciatic DRG before and 3 days after SNI. Scale bar, 50 μm. (**E**) Fold change of MHC I expression shown in (D) (n = 3). (**F**) Percentage of antigen-presenting (AP) DRG neurons (n = 3). (**G**) Representative MHC I or cleaved caspase 3 (cl-cas3) coimmunostaining with luciferase (Lu) and DAPI in DRG after AAV-rtTA or AAV-GAr-rtTA and 3 days after SNI. Scale bar, 50 μm. (**H**) Fold change of MHC I and cleaved caspase 3 expressions in DRG shown in (G) (n = 6). (**I**) SCG10 immunostaining of sciatic nerves from AAV-rtTA– or AAV-GAr-rtTA– infected aged mice 3 days after SNI. The dashed line indicates the proximal injury site. Scale bar, 500 μm. (**J**) Normalized SCG10 intensity to the proximal crush site (n = 6). (**K**) Representative coimmunostaining of cleaved caspase 3, Tuj1, and DAPI in DRG before and 3 days after SNI. Scale bar, 50 μm. (**L**) Quantification of the percentage of cleaved caspase 3–positive DRG neurons (n = 4). (**M**) Immunoblot shows p-AKT, AKT, p-S6, S6, and Tuj1 expression in the sciatic DRG after control IgG or CD8 mAb 3 days after SNI. (**N**) Immunoblot quantification of p-AKT/AKT and p-S6/S6 in the sciatic DRG (n = 4). $^{*}P < 0.05$, $^{**}P < 0.01$, $^{***}P < 0.001$, $^{****}P < 0.0001$ [two-way ANOVA with post hoc Sidak's test in (B) and (J); unpaired Student's t test in (C) and (H); one-way ANOVA with post hoc Tukey's test in (E), (F), (L), and (N)]. Data are means ± SEM and represent two [(B), (C), (L), and (N)] or three [(E), (F), (H), and (J)] experiments.

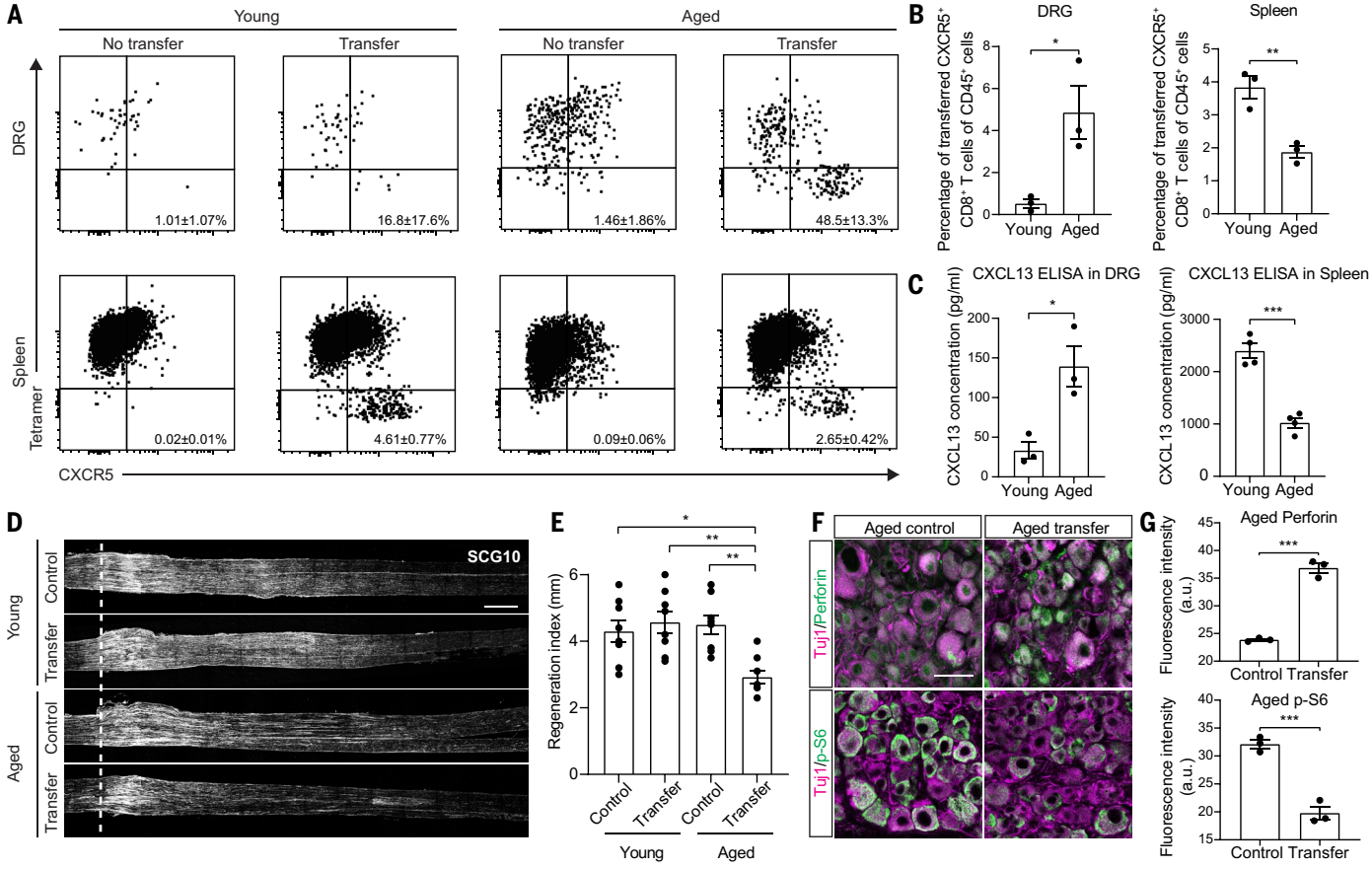

Fig. 5. CXCR5$^+$CD8$^+$ T cells cause aging-dependent regenerative decline after SNI. (**A**) Representative flow cytometry plots of endogenous and transferred CXCR5$^+$CD8$^+$ T cells (gated TCRβ$^+$CD8$^+$ cells) from the sciatic DRG and spleen of OT-I *Rag2*$^{-/-}$ mice 3 days after SNI. Tetramer (SIINFEKL) was used to distinguish the host OT-I CD8 T cells from donated wild-type CD8 T cells. (**B**) Quantification of transferred CXCR5$^+$CD8$^+$ T cells from DRG or spleen 3 days after SNI (n = 3). (**C**) CXCL13 ELISA from OT-I *Rag2*$^{-/-}$ DRG or spleen (n = 3 or 4). (**D**) Representative SCG10 immunostaining of sciatic nerves with or without CXCR5$^+$CD8$^+$ T cell transfer 3 days after SNI in OT-I *Rag2*$^{-/-}$ mice. The dashed line indicates the proximal injury site. Scale bar, 500 μm. (**E**) Analysis of regeneration index (n = 6 or 8). (**F**) Perforin or p-S6 counterstained with Tuj1 in the DRG from aged OT-I *Rag2*$^{-/-}$ mice 3 days after SNI with or without CXCR5$^+$CD8$^+$ T cell transfer. Scale bar, 50 μm. (**G**) Quantification of perforin or p-S6 normalized intensity (n = 3). *P < 0.05, **P < 0.01, ***P < 0.001 [one-way ANOVA with post hoc Tukey's test in (E); unpaired Student's t test in (B), (C), and (G)]. Data are means ± SEM and represent three experiments.

of CXCR5$^+$CD8$^+$ cells to DRG (Fig. 6, A to E) and the spleen (Fig. 6, I and J). Sciatic nerve regeneration was significantly enhanced by CXCL13 antagonism after adoptive transfer of wild-type CD8$^+$ T cells (Fig. 6, F to H), but not of *Cxcr5*$^{-/-}$ CD8$^+$ T cells, which were also associated with higher regeneration relative to wild-type CD8$^+$ T cells (Fig. 6, F to H). Thus, CXCL13 acting on its receptor CXCR5 is required for CD8 T cell migration and to restrict sciatic nerve regeneration in aged DRG.

CXCL13 neutralization reverses aging-dependent regenerative decline and promotes neurological functional recovery after sciatic nerve injury

Finally, we investigated whether CXCL13 neutralization promotes axonal regeneration, epidermal innervation, and functional recovery in aged animals. Injection of CXCL13 mAb significantly enhanced neurite outgrowth in DRG ex vivo culture, reduced the recruitment of CXCR5$^+$ T and B cells, and blocked aging-dependent regenerative failure of sciatic nerve and DRG infiltration of CD8 T cells 3 days after SNI in aged mice but had no effect in young mice (Fig. 7, A to E, and fig. S18, A to F). However, CXCL13 neutralization did not alter the number of CD11b$^+$F4-80$^+$ macrophages in DRG (fig. S19).

In a separate experiment, we tested the effects of CXCL13 antagonism on functional recovery. Aged mice recovered significantly more slowly than young mice, and CXCL13 neutralization induced a significantly accelerated recovery in aged mice in all the sensory modalities investigated (Fig. 7, F to I, and fig. S18, G to I). CXCL13 neutralization promoted significant skin reinnervation from the hairless interdigital area of the hindpaw in aged mice (Fig. 7, J and K, and fig. S18, J and K). Thus, CXCL13 neutralization promotes axonal regeneration, skin reinnervation, and functional recovery in aged animals.

Discussion

Our work indicates that aging primes DRG neurons for regenerative failure after axonal injury by a CXCL13-dependent mechanism that regulates CXCR5$^+$CD8$^+$ T cell entry into the DRG. Regenerative failure is a consequence of the CXCL13-dependent DRG recruitment of CXCR5$^+$CD8$^+$ T cells that communicate with DRG neurons via MHC I on the neuronal cell surface to drive regenerative inhibitory signaling. Unlike in the aged DRG tissue microenvironment, young adult DRG do not harbor T cells before an injury and the T cells do not colonize the DRG parenchyma until many days after nerve injury, past the initiation of the axonal regenerative response (*19*). CXCL13 neutralization reduced the number of CXCR5$^+$CD8$^+$ T cells into the DRG, allowing for significantly

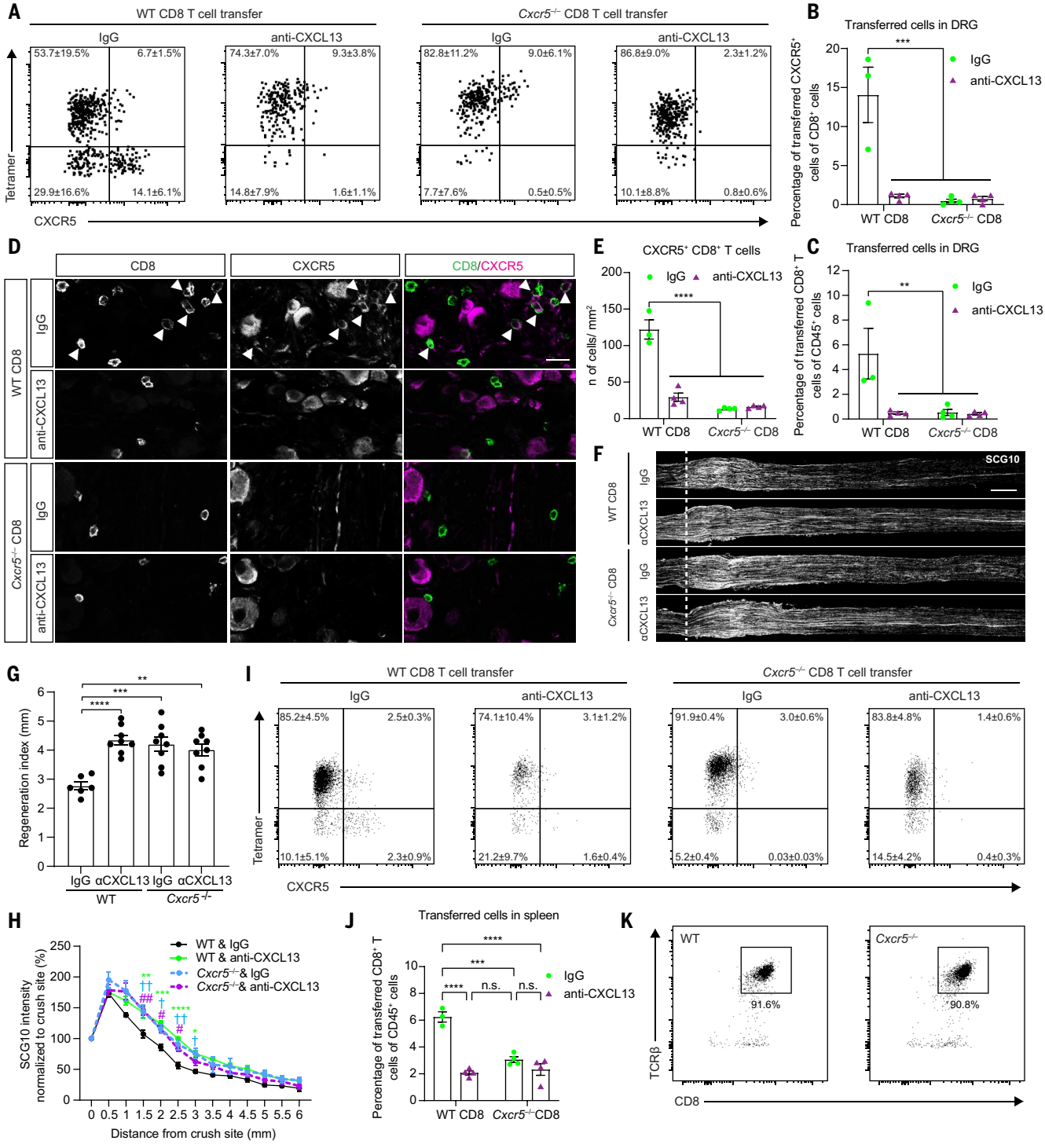

Fig. 6. CXCR5 is required for CD8 T cell infiltration in aged DRG and regenerative decline after SNI. (**A**) Representative flow cytometry plots of endogenous and transferred CXCR5$^+$CD8$^+$ T cells (gated TCRβ$^+$CD8$^+$ cells) from the sciatic DRG of OT-I *Rag2*$^{-/-}$ aged mice 3 days after SNI and treatment with IgG or CXCL13 mAb. (**B**) Quantification of transferred CXCR5$^+$CD8$^+$ T cells from DRG shown in (A) (n = 3 or 4). (**C**) Quantification of transferred CD8$^+$ T cells from DRG (n = 3 or 4). (**D**) Representative coimmunostaining of CD8 and CXCR5 in sciatic DRG 3 days after SNI. Scale bar, 10 μm. (**E**) Quantification of the number of CXCR5$^+$CD8$^+$ T cells in sciatic DRG (n = 4). (**F**) Representative SCG10 immunostaining of sciatic nerves after control IgG or CXCL13 mAb treatment 3 days after SNI. The dashed line indicates the proximal injury site. Scale bar, 500 μm. (**G**) Analysis of regeneration index (n = 6 or 8). (**H**) Normalized SCG10 intensity to the proximal crush site (n = 6 or 8). *P < 0.05, **P < 0.01, ***P < 0.001, ****P < 0.0001 (wild-type & anti-CXCL13 versus wild-type & IgG); †P < 0.05, ††P < 0.01 (CXCR5$^{-/-}$ & IgG versus wild-type & IgG); #P < 0.05, ##P < 0.01 (CXCR5$^{-/-}$ & anti-CXCL13 versus wild-type & IgG). (**I**) Representative flow cytometry plots of endogenous and transferred CD8$^+$ T cells (gated TCRβ$^+$CD8$^+$ cells) from splenocytes from OT-I *Rag2*$^{-/-}$ aged mice 3 days after SNI with control IgG or CXCL13 mAb. (**J**) Percentage of transferred CD8$^+$ T cells from spleen (n = 3 or 4). (**K**) Plots showing wild-type or *Cxcr5*$^{-/-}$ CD8$^+$ T cells after sorting. *P < 0.05, **P < 0.01, ***P < 0.001, ****P < 0.0001 [one-way ANOVA with post hoc Tukey's test in (B), (C), (E), (G), (H), and (J)]. Data are means ± SEM and represent four experiments.

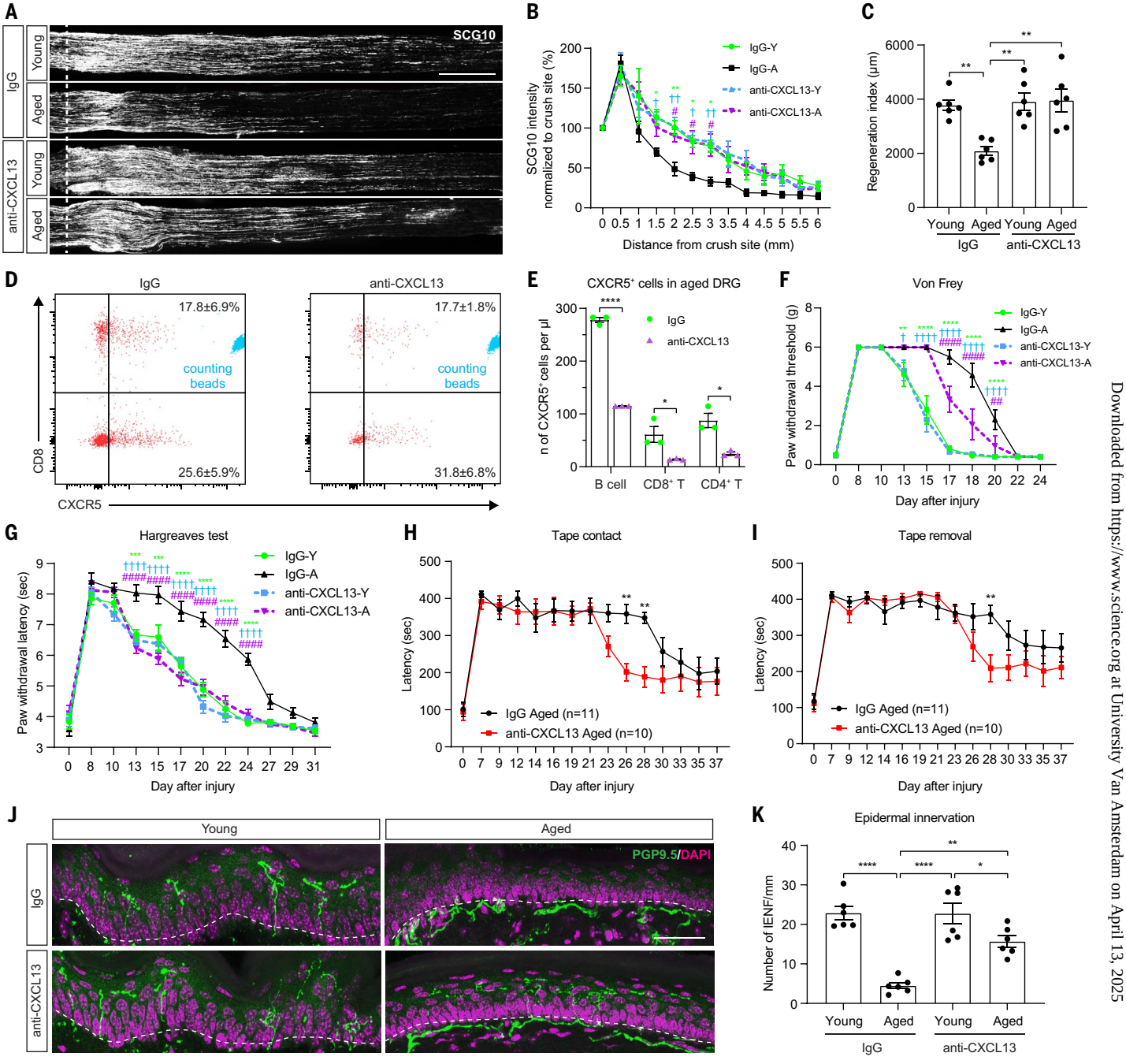

Fig. 7. CXCL13 neutralization enhances axonal regeneration, epidermal reinnervation, and sensory functional recovery after SNI in aged mice. (**A**) Representative SCG10 immunostaining of sciatic nerves after control IgG or CXCL13 mAb treatment 3 days after SNI. The dashed line indicates the proximal injury site. Scale bar, 500 μm. (**B**) Normalized SCG10 intensity (n = 6, *P < 0.05, **P < 0.01, IgG-Y versus IgG-A; †P < 0.05, ††P < 0.01, anti-CXCL13-Y versus IgG-A; #P < 0.05, anti-CXCL13-A versus IgG-A). (**C**) Analysis of regeneration index (n = 6). (**D**) Representative flow cytometry plots of CXCR5$^+$ and CD8$^+$ T cells (gated CD45$^+$TCRβ$^+$CD19$^-$ cells) from the sciatic DRG of aged mice 3 days after SNI. (**E**) Quantification of CXCR5$^+$ B, CD8$^+$, and CD4$^+$ T cell number from DRG 3 days after SNI (n = 3). (**F** and **G**) Mechanical sensitivity by von Frey test (F) and thermosensitivity analysis by Hargreaves test (G) after SNI. **P < 0.01, ***P < 0.001, ****P < 0.0001 (IgG-Y versus IgG-A); †P < 0.05, ††††P < 0.0001 (anti-CXCL13-Y versus IgG-A); ##P < 0.01, ####P < 0.0001 (anti-CXCL13-A versus IgG-A) (n = 10 or 11; two-way ANOVA with post hoc Sidak's test). (**H** and **I**) Sensory responses by adhesive tape contact (H) and removal (I) test after SNI (n = 10 or 11). (**J**) Representative coimmunostaining of PGP9.5 and DAPI shows the epidermal innervation of the hindpaw interdigital skin 18 days after SNI. The dashed lines indicate the boundary of the epidermis and dermis. Scale bar, 50 μm. (**K**) Quantification of the number of intra-epidermal nerve fibers (IENF) per mm of interdigital skin (n = 6). *P < 0.05, **P < 0.01, ***P < 0.001, ****P < 0.0001 [two-way ANOVA with post hoc Sidak's test in (B), (F), (G), (H), and (I); one-way ANOVA with post hoc Tukey's test in (C) and (K); unpaired Student's t test in (E)]. Data are means ± SEM and represent three [(B), (C), and (E)] or two [(F), (G), (H), (I), and (K)] experiments.

enhanced axonal regeneration and sensory recovery.

CXCL13 is typically expressed in lymphoid organs to control the recruitment of B cells and antigen-presenting cells (*20*). The CXCL13 receptor CXCR5 is highly expressed by a subset of B cells and by $CD4^+$ T cells that are attracted to CXCL13-rich sites such as the lymphoid tissue. CXCL13 has also been found to be expressed by astrocytes and DRG neurons regulating pain (*21*, *22*). $CXCR5^+CD8^+$ T cells have been described as follicular effector memory T cells and have been implicated in the orchestration of the follicular T and B cell responses to infection (*23*, *24*). Clonally expanded $CD8^+$ T cells are present in neurogenic niches in the aged mouse brain whose activity is required to inhibit neural stem cell proliferation (*25*). However, the role of $CD8^+$ T cells in the nervous system can be either neurotoxic or neuroprotective, depending on the specific experimental conditions (*26*–*28*).

We also observed that $CXCR5^+$ B cells are attracted by CXCL13 gradients toward the DRG in aged animals and after CXCL13 overexpression, but remain trapped in the perivenular space. Unlike $CXCR5^+CD8^+$ T cells, $CXCR5^+$ B cells do not migrate into the parenchyma and do not affect neuronal regenerative ability. Whether CXCL13 and $CXCR5^+$ B and T cells populate the perivenular spaces or the parenchyma in the aged brain and whether they may contribute to tissue damage remains unexplored.

$CXCR5^+CD8^+$ T cells are recruited and progressively accumulate into the DRG, where they reside until they act as effector T cells upon MHC I antigen presentation by injured neurons. Although the nature of the aging and injury-dependent antigens remains elusive, we speculate that the combination of injury-dependent antigens with viral peptides accumulated and processed during the lifespan may lead to T cell–dependent neuronal MHC I recognition and inhibition of axonal regeneration after injury.

Neuronal MHC I has been implicated in synaptic maintenance of sciatic motor neurons and locomotor function after sciatic nerve or spinal cord injury in young animals (*29*, *30*). However, its role in axonal regeneration of aged sensory neurons had not been explored. Here, we have shown that the inhibitory signaling limiting axonal regeneration in aged DRG neurons appears to rely on neuronal MHC I–$CD8^+$ T cell interactions that elicit intracellular signals such as perforin, granzyme B, and caspase 3 activation (*31*–*33*). Active caspase 3 is needed to reduce pAKT, likely by AKT cleavage (*15*), resulting in decrease of downstream signals. Depletion of $CD8^+$ T cells or inhibition of caspase 3 activation counteracts aging-dependent regenerative decline and results in a significant increase in both pAKT and pS6. These are strongly developmentally regulated signals within the regenerative PI3K and mTOR pathways (*17*). Thus, the induction of these pathways in aged DRG neurons is likely to be crucial to promote regenerative signaling and merits further exploration.

In line with our data, CXCL13 expression was previously shown to be reduced in the spleens and lymph nodes of aged mice relative to young mice (*34*, *35*), leading to reduced accumulation of B and T cells. The CXCL13-dependent shift of B cells and T cells from secondary lymphoid organs to peripheral tissues may be a general phenomenon leading to tissue damage beyond the peripheral nervous system.

The delivery of CXCL13 mAbs that promote axonal regeneration, skin reinnervation, and recovery of neurological function represents a translational opportunity for improving repair after injury. CXCL13 neutralization may reduce $CXCR5^+$ follicular helper B cell and T cell homing, with a risk of increased susceptibility to viral infection. However, the CXCL13 mAb used here is currently in preclinical development and has been effective in ameliorating pathology and disability in animal models of rheumatoid arthritis and multiple sclerosis without obvious toxicity (*36*). Our results therefore suggest that CXCL13 neutralization may be considered for the treatment of axonal injuries affecting the elderly. More generally, they describe aging-specific regenerative mechanisms, suggesting the need for targeted interventions that consider age at the time of injury or disease initiation.

Materials and methods

Mice

Wild-type 8- to 10-week-old C57BL/6J young mice were obtained from Charles River, whereas 20- to 22-month-old aged mice were supplied by either Charles River or by M. Jucker (Hertie Institute for Clinical Brain Research, University Hospital Tübingen, Germany). OT-I *Rag2*$^{-/-}$ mice on a C57BL/6 genetic background were provided by M. Botto (Imperial College London). *Cxcr5*$^{-/-}$ mice on a C57BL/6 genetic background were donated by T. Arnon (University of Oxford). All animal procedures were performed in accordance with the UK Animals Scientific Procedures Act (1986) and approved by the ethical committee of Imperial College London.

DRG cell culture

Sterile 15-mm glass coverslips in 24-well plates were coated with 0.003% poly-L-ornithine (Sigma) diluted in H_2O for 1 hour at 37°C. After three washes with water, the coverslips were coated with laminin (1 μg/ml; Millipore) prepared in PBS (Invitrogen) for 3 hours at room temperature. After two washes with PBS, the wells were filled with DMEM and placed at 37°C until cells were plated. DRGs were dissected and collected in Hank's balanced salt solution (HBSS; Invitrogen) on ice. HBSS was then removed and replaced with 500 μl of digest solution [Dispase II (5 mg/ml, Sigma) and 2.5 mg/ml collagenase type II (2.5 mg/ml, Worthington] in DMEM (Invitrogen) for 40 min in a 37°C water bath with gentle tube flicks every 5 min. DRG were collected by centrifugation at 72*g* for 2 min after digestion and washed once with warm DRG medium [DMEM/F12 (Invitrogen), 1× B27 (Invitrogen), and 10% fetal bovine serum (FBS; Sigma)]. DRG were then resuspended in 1 ml of warm DRG medium and dissociated by pipetting with fire-polished Sigmacote (Sigma)–coated glass pipette 15 times. Undissociated tissue was filtered with a 100-μm cell strainer (BD Falcon) and cells were counted under a bright-field microscope with a hemocytometer. After cell counting, cells were centrifuged, resuspended with warm DRG culture medium [DMEM/F12 (Invitrogen), 1× B27 (Invitrogen), and 1% penicillin and streptomycin (Invitrogen)] and plated (4000 cells per well). The DRG cells were cultured at 37°C in 5% CO_2 for 24 hours.

DRG neurite outgrowth analysis

The average neurite length of cultured DRG cells was measured by using Neurolucida software (MBF Bioscience) with at least 100 cells (five fields per coverslip randomly selected) per condition in technical and biological triplicate.

Immunocytochemistry

Cultured DRG cells were fixed with ice-cold 4% paraformaldehyde (PFA; Sigma) in 1× PBS for 30 min on ice and washed with 1× PBS three times. Cells were blocked in 1× PBS, 0.1% Triton X-100 (Sigma), and 5% normal goat serum (Abcam) at room temperature for 1 hour followed by the incubation with primary antibodies in 1× PBS, 0.1% Triton X-100, and 2% normal goat serum overnight at 4°C. Cells were then washed three times with 1× PBS and incubated with secondary antibodies in 1× PBS, 0.1% Triton X-100, and 2% normal goat serum for 2 hours at room temperature in the dark. Cells were washed three times with 1× PBS and incubated with 4,6-diamidino-2-phenylindole (DAPI, ThermoFisher, 62248, 0.2 μg/ml) in 1× PBS, 0.1% Triton X-100 for 10 min followed by two washes with 1× PBS. The coverslips with cells facing down were transferred and mounted with Antifade mounting medium (Vectashield, H-1000) on the slides. Detailed antibody information is provided in table S1.

Immunohistochemistry

Mice were anesthetized by ketamine-xylazine mixture (80 mg of ketamine and 10 mg of xylazine per kilogram of body weight) via intraperitoneal (i.p.) injection and transcardially perfused with 20 ml of ice-cold PBS

followed by 4% PFA in a flow rate of 5 ml/min. DRG, sciatic nerves, or glabrous skin of hindpaws were excised and post-fixed in 4% PFA for 2 hours on ice and transferred to 30% sucrose (Sigma) for 3 days prior to embedding in OCT compound (Tissue-Tek). DRG were sectioned at 10 μm, sciatic nerves at 12 μm, and interdigital footpads at 30 μm perpendicularly to the skin surface with a cryostat (Leica). Sections were treated with a blocking solution containing 10% normal goat serum or normal donkey serum (Abcam) and 0.3% Triton X-100 in PBS for 1 hour at room temperature and stained with primary antibodies at 4°C overnight. Sections were washed with 1× PBS three times followed by secondary antibody incubation at room temperature for 2 hours. Sections were then stained with DAPI (ThermoFisher, 62248, 0.2 μg/ml) for 15 min at room temperature followed by three washes with 1× PBS and then mounted with Antifade mounting medium (Vectashield, H-1000). DRG were imaged with a Nikon Eclipse TE2000 microscope using 20× magnification (DIC Plan-Apochromat VC objective and QImaging OptiMOS detection system). Sciatic nerves (20× magnification, HC Plan-Apochromat CS2) and epidermis (40× magnification with oil lens, HC Plan-Apochromat CS2) were imaged with a Leica TCS SP8 confocal laser scanning microscope in Leica DFC9000 GTC detection system. Detailed antibody information is provided in table S1.

Sciatic nerve crush injury

Sciatic nerve was crushed following the protocol previously described (*37*). Mice were anesthetized with 2% isoflurane in oxygen (1 liter/min) and injected with buprenorphine (0.1 mg/kg body weight) and rimadyl (5 mg/kg body weight) subcutaneously (s.c.) for analgesia. An incision across the mid-thigh was made in the skin, the sciatic nerve was exposed by opening the fascial plane, and a small deeper incision was made between the gluteus maximus and the anterior head of the biceps femoris. The proximal side of exposed nerve where the three fascicles are sequentially aligned was placed on the bottom jaw of a super-fine hemostatic forceps (Fine Science Tools, 13020-12) 1.5 mm from their tip. The nerve was crushed for 30 s at three clicks of the forceps with no nerve stretch. The skin was then closed with suture clips. Mice were administered buprenorphine (0.1 mg/kg body weight) twice per day and rimadyl (5 mg/kg body weight) daily by s.c. injection for 3 days post-operation. Sham surgery was performed to expose the nerves without injury.

Retrograde tracing after nerve injury

Mice were anesthetized following the protocol of sciatic nerve crush injury. The skin and muscle at the distal thigh were opened to expose the nerve and 1 μl of 1% Alexa Fluor 555-conjugated cholera toxin subunit B (CTB, ThermoFisher) diluted in sterile saline was injected in the nerve 8 mm distal to the injury site with Hamilton syringe and needle (NDL small RN ga34/15mm/pst45°) (Hamilton) as described (*38*). The skin was closed with suture clips.

RNA preparation and sequencing

RNA sequencing was performed using RNA from the whole sciatic DRG tissue of young or aged mice 24 hours after sham or sciatic nerve injury. Specifically, sciatic DRG were dissected from one mouse per sample and stored in RNAlater stabilization solution (ThermoFisher). Tissue was homogenized with RNase free micro pestle and RNA was extracted using RNeasy kit (Qiagen) following the manufacturer's protocol. On-column DNase digestion was performed with the RNase-free DNase set (Qiagen) for 15 min to remove DNA. RNA concentrations and purity were measured using Agilent 2100 Bioanalyzer (Agilent). RNA with RNA integrity number (RIN) above 7.5 was used for library preparation. Libraries were prepared at Ospedale San Raffaele (Milan) using the TruSeq mRNA Sample Preparation kit (Illumina) and sequenced using Illumina HiSeq 2500 100-cycle, paired-end sequencing.

Bioinformatic analysis

RNA sequencing data analysis was performed as published (*39*). FDR-corrected *P* value was implemented with Benjamini-Hochberg (BH) correction. DE genes (FDR < 0.05) of three comparisons (SNI Young, Sham Aged, and SNI Aged versus Sham Young, respectively) were analyzed for Gene Ontology (GO) and KEGG pathways using DAVID v6.7 (https://david-d.ncifcrf.gov/) with all expressed genes in our dataset as the background. The categories of GO and KEGG pathways were selected by $P < 0.01$ for both up- and down-regulation. Area proportional Venn diagrams were generated using Biovenn (www.biovenn.nl/). The differentially up-regulated genes from SNI Aged versus Sham Young involved in immune response collected from GO and KEGG pathways were analyzed for protein-protein network established by STRING (https://string-db.org/). The stringent criteria were selected using the active interaction sources of experiments and databases, as well as the highest confidence of the minimum required interaction score. The network was visualized by Cytoscape v3.7.2 (https://cytoscape.org/). For the generation of Circos plots of VJ segment usage, we used MiXCR (v3.0.13) to identify T cell receptor clonotypes from whole DRG RNA-seq data. MiXCR's "analyze shotgun" method was run directly on the fastq files from the RNA-seq experiment using default parameters for mouse RNA to identify clonotypes. The T cell receptor clonotypes were then pooled among replicates and imported to VDJtools v1.2.1. The "PlotFancyVJUsage" method was used to generate the Circos plot separately for each biological condition, using default parameters.

CXCL13 ELISA assay

Sciatic DRG dissected from two young or aged mice per sample 3 days after sham or sciatic nerve injury were collected and homogenized in 150 μl Assay Diluent A supplied from Mouse CXCL13 ELISA kit (ThermoFisher) with protease inhibitors (Roche) to produce the data in Fig. 1I. Total DRG and spleen were dissected from one young or aged OT-I $Rag2^{-/-}$ mouse per sample and homogenized in 150 μl and 2 ml of Assay Diluent A buffer with protease inhibitor, respectively, to produce the data in Fig. 5C. After homogenization, Triton X-100 was added to a final 1% concentration. Samples were frozen in liquid nitrogen and thawed followed by centrifugation at 10,000*g* for 5 min to remove the debris. Protein concentration was quantified using BCA protein assay kit (ThermoFisher) and 100 μl of cell lysate was used for the CXCL13 ELISA assay using Mouse CXCL13 ELISA kit according to the manufacturer's protocols. CXCL13 ELISA measurements were obtained by measuring absorbance on an ELISA plate reader set at 450 nm and subtracting 550-nm values to correct for optical imperfections in the microplate. CXCL13 concentrations in the cell lysate were calculated according to the standard curve.

Quantification of immunostaining

Arbitrary fluorescence intensity was measured with ImageJ software (NIH) and normalized fluorescence intensity was calculated by subtracting the intensity of the background immunofluorescent signal. The relative fold change was calculated by comparing the normalized fluorescence intensity of the experimental group versus the control group. The cells designated positive for the expression of cleaved caspase 3, perforin, and granzyme B showed fluorescence intensity at least twofold above background. Longitudinal sections of sciatic nerve stained with SCG10 were analyzed for axonal regeneration. SCG10 arbitrary intensity was measured along the nerve and percentage of intensity in every 0.5 mm was quantified away from the proximal site of crush. A regeneration index was evaluated by calculating the distance away from the proximal injury site where the intensity was reduced to 50% level with respect to the proximal site. For epidermal and dermal reinnervation, the number of IENF indicated by PGP9.5 staining from sagittal sections of the skin was measured per unit of volume. Animals were randomly and equally grouped.

Immunoblotting

Sciatic DRG were dissected and collected in 1× PBS with protease inhibitor (Roche) and

phosphatase inhibitor (Roche). Tissues were then homogenized, and protein lysate was extracted by RIPA buffer. Protein concentration was measured with BCA protein assay kit (ThermoFisher) and 20 μg of protein was loaded to 10% SDS-PAGE gel and transferred on nitrocellulose membrane of iBlot Transfer Stack (ThermoFisher) by iBlot 2 Gel Transfer Device (ThermoFisher) under the default P0 program. The membrane was blocked with 5% milk in TBST buffer for 1 hour at room temperature (RT) and incubated with primary antibodies at 4°C overnight. The membranes were then washed with TBST and incubated with horseradish peroxidase (HRP)–conjugated secondary antibodies at RT for 1 hour followed by chemiluminescent detection with Amersham Hyperfilm (GE Healthcare Life Sciences) after incubation with ECL substrate (ThermoFisher). Detailed antibody information is provided in table S1.

Flow cytometry

For cell characterization in vivo, young or aged naïve or sciatic nerve-injured animals were injected with 3 μg of APC-conjugated anti-CD45 (I3/2.3, Biolegend) intravenously (i.v.) for 3 min. Peripheral blood or DRG were collected in 10 ml of 1× PBS with 2 mM EDTA and RPMI-1640 medium (ThermoFisher), respectively, after anesthesia. Blood cells were collected by centrifugation at 300*g* for 5 min at RT and erythrocytes were lysed using 1× RBC lysis buffer (Biolegend). Cells were washed with 1× PBS three times and filtered by 70-μm cell strainer (Corning) to remove the clumps and resuspended by fresh FACS buffer (0.5% BSA and 2 mM EDTA in PBS) for staining. DRG were washed by 1× PBS once and dissociated with digestion buffer [CLSPA (0.5 mg/ml, Worthington, #LS005273)] and DNase I (7.5 μg/ml, Roche, #10104159001) in RPMI-1640 at 37°C for 30 min. After digestion, DRG tissues were dispersed and filtered through a 70-μm cell strainer to collect the single-cell suspension and washed with rinse buffer (5% FBS in RPMI-1640). After centrifugation, the pellet was resuspended with 1 ml of DNase solution [250 μg/ml of DNase I in 1× DNase buffer (1.21 mg/ml of Tris Base, 0.5 mg/ml of $MgCl_2$, and 73 μg/ml of $CaCl_2$ in RPMI-1640)] at RT for 30 min. Cells were washed with FACS buffer for staining.

Isolated cells from the blood and DRG samples were treated with 1.0 μg of TruStain FcX anti-mouse CD16/32 antibody (Biolegend) per 10^6 cells in a 100-μl volume to block Fc receptors for 10 min on ice and stained with primary antibodies in FACS buffer with Brilliant Stain Buffer (BD Horizon). LIVE/DEAD Fixable Aqua Dead Cell Stain Kit (ThermoFisher) was also used to exclude the dead cells from staining. Cells were stained with the cocktail antibodies at 4°C in the dark for 20 min and stained with PE-streptavidin (2 μg/ml, Biolegend) at 4°C for 20 min after washing. Fluorescence Minus One (FMO) and PE-streptavidin staining controls were used for the gating boundaries. To minimize anti-CXCR5 shedding before cell acquisition, stained cells were immediately fixed with IC fixation buffer (ThermoFisher) for 20 min at RT. Cells were washed with 1× PBS and resuspended with 180 μl of FACS buffer. Precision Counting Beads (20 μl; Biolegend, 424902) were added to each sample before cell acquisition by flow cytometer LSR II (BD Biosciences). All DRG cells and 5000 blood cells or splenocytes were acquired for quantification. Detailed antibody information is provided in table S1.

NF-κB and Cxcl13 expression in cultured DRG neurons

Isolated DRG primary cells were plated with cytokines and incubated at 37°C in 5% CO_2 for 24 hours. The following compounds were used in cell culture: recombinant mouse TNF-α (410-MT, R&D Systems, 500 pg/ml), recombinant mouse IL-1β (401-ML, R&D Systems, 600 pg/ml), recombinant mouse BAFF (8876-BF, R&D Systems, 100 ng/ml), and recombinant mouse lymphotoxin α1/β2 (9968-LY, R&D Systems, 100 ng/ml). Selective IKK inhibitor (10 μM; PS1145, TOCRIS, #4569) was in turn used with or without lymphotoxin α1/β2 stimulation for 24 hours. Total RNA from cultured cells was extracted using RNeasy kit (Qiagen) according to manufacturer's guidelines. cDNA was then synthesized with SuperScript II Reverse Transcriptase (ThermoFisher). qRT-PCR was performed using KAPA SYBR FAST qPCR kit (Sigma, KK4601) from Applied Biosystems 7900 Real-Time PCR System. Ct values normalized versus *Gapdh* as a housekeeping gene were exported and relative fold change of gene expression compared to vehicle control was calculated by $2^{-\Delta\Delta Ct}$. Primers used in qPCR were as follows: *Nfκb1* forward 5′-GAAATTCCTGATCCAGACAAAAAC-3′ and reverse 5′-ATCACTTCAATGGCCTCTGTGTAG-3′, *Nfκb2* forward 5′-GGCCGGAAGACCTATCCTACT-3′ and reverse 5′-CTACAGACACAGCGCACACT-3′, *Cxcl13* forward 5′-CTCTCCAGGCCACGGTATT-3′ and reverse 5′-TAACCATTTGGCACGAGGAT-3′, *Gapdh* forward 5′-TCAACAGCAACTCCCACTCTTCCA-3′ and reverse 5′-ACCCTGTTGCTGTAGCCGTATTCA-3′.

Cell migration in culture after CXCL13 overexpression

AAV5-GFP (Vector Biolabs, #7073) or AAV5-*Cxcl13*-GFP (AAV-256398) was added (1 μl per well) to DRG primary cell culture (8000 cells per well in 24-well plates) for a 5-day incubation. Thereafter, culture medium was collected and centrifugated at 300*g* for 5 min and 200 μl of culture medium was transferred to each receiving well of Corning HTS Transwell 96-well permeable supports, 5.0-μm pore size (Sigma, CLS3387). A fresh wild-type mouse spleen was meshed on 70-μm cell strainer and collected cells were treated with RBC lysis buffer to remove the erythrocytes. Purified splenocytes after PBS washing were incubated with 250 μg/ml of DNase I for 30 min at RT. After DNA digestion and PBS washing, cell numbers were counted and adjusted to the density of 5×10^5 cells per 100 μl by DRG culture medium. Cell suspension (100 μl per well) was carefully loaded to the transwell, which was then placed onto the receiving plate to make sure the liquid from each well was in contact with the transwell. The plate was incubated at 37°C for 4 hours. After migration, the transwell was removed and the medium in the receiving plate was collected. The medium was pooled from six wells as one sample. Cells were stained and acquired by flow cytometer and three replicates per group were measured for quantification.

To validate the successful overexpression or secretion of CXCL13 in cell culture, total RNA was extracted for cDNA synthesis followed by *Cxcl13* qRT-PCR and DNA electrophoresis, or culture medium was collected for CXCL13 assay using mouse CXCL13 ELISA kit as described above.

In vivo DRG neuron CXCL13 overexpression

Eight-week-old mice were anesthetized with 2% isoflurane in 1 liter/min oxygen and administered with buprenorphine (0.1 mg/kg body weight) and rimadyl (5 mg/kg body weight) by s.c. injection. The skin and muscle at the distal thigh were opened to expose the nerve, and 2 μl of AAV-GFP or AAV-CXCL13-GFP were injected in the nerve bilaterally at the distal site of the thigh with Hamilton syringe and needle (NDL small RN ga34/15mm/pst45°) (Hamilton). The skin was closed with suture clips. Animals were monitored for 6 weeks after CXCL13 overexpression. Recombinant mouse IFN-γ (10 μg, Biolegend, #575308) and 25% D-mannitol (200 μl, Sigma, M4125) were i.p. and i.v. injected, respectively, into each mouse 2 days before sciatic nerve crush. Sciatic DRG were collected for tissue dissociation with CLSPA and cells were then stained with LIVE/DEAD-Aqua and cell markers for flow cytometry. Sciatic DRG and nerves were collected and fixed for the measurement of gene overexpression and axonal regeneration.

Cell depletion experiments

To deplete $CD8^+$ or $CD4^+$ T cells in vivo, 22- to 24-month-old mice were i.p. injected with 200 μg of anti-mouse CD8α (YTS 169.4, BioXcell, BE0117) or anti-mouse CD4 (YTS 191, BioXcell, BE0119). An equivalent amount of rat IgG2b (LTF-2, BioXcell, BE0090) was injected into the control group of animals. Depletion of B cells was performed following a

strategy described previously (*40*). Aged mice were i.p. injected with antibody cocktail consisting of 150 μg of InvivoMAb anti-mouse CD19 (1D3, BioXcell, BE0150), 150 μg of InvivoMAb anti-mouse B220 (RA3.3A1/6.1, BioXcell, BE0067), and 150 μg of InvivoMAb anti-mouse CD22 (Cy34.1, BioXcell, BE0011). Forty-eight hours later, the mice were injected with a secondary antibody InvivoMAb anti-rat kappa (MAR18.5, BioXcell, BE0122), at a dose of 150 μg per mouse. Rat IgG2a (2A3, BioXcell, BE0089), polyclonal rat IgG (BioXcell, BE0094), mouse IgG1 (MOPC-21, BioXcell, BE0083), and mouse IgG2a (C1.18.4, BioXcell, BE0085) isotype controls were injected in the same dosage. All injections were performed twice 1 week prior to the sciatic nerve injury and once more the day after injury.

DRG neuron and OT-I CD8$^+$ T cell coculture

Eight-week-old wild-type mice were injected with PBS or 10 μg of recombinant mouse IFN-γ 2 days before being killed for DRG dissection and DRG neuron culture. Naïve OT-I CD8$^+$ T cells were purified from 8-week-old OT-I mice using the MojoSort Mouse CD8 T Cell Isolation kit (Biolegend). Purified live CD8$^+$ T cells were counted by Trypan Blue (ThermoFisher) staining. Approximately 4000 DRG neurons per well were plated with 10,000 OT-I CD8$^+$ T cells with or without $OVA_{257–264}$ peptide (100 nM, SIINFEKL, InvivoGen) at 37°C for 24 hours. The culture medium was then removed and the cells were fixed with 4% PFA. This was followed by two washes with 1× PBS for immunostaining.

GAr-rtTA–mediated immune evasion

AAV5-rtTA or AAV5-GAr-rtTA viral particles, which were provided by J. Verhaagen (Netherlands Institute for Neuroscience), were mixed with the viral particles expressing doxycycline-inducible luciferase (AAV5-dox-i-luciferase) in a 1:1 ratio to be titer-matched by PBS+5% sucrose dilution. Viral mix (3 μl) was injected into the sciatic nerve of aged mice bilaterally. Five weeks later, doxycycline (Stemcell, #72742) reconstituted in PBS was delivered by daily i.p. injection at a dosage of 50 mg/kg body weight for 1 week before sciatic nerve injury and 3 days after injury. Upon killing, sciatic DRG and nerves were dissected for immunostaining.

CXCL13 neutralization

CXCL13 mAb (5378) and control IgG2a mAb (2510) were kindly supplied by Vaccinex Inc. (Rochester, NY). For DRG ex vivo culture, young and aged mice were treated with control IgG or CXCL13 mAb (30 mg/kg body weight, i.p.) three times 1 week before DRG dissection and primary cell culture. Isolated DRG cells were incubated at 37°C in 5% CO_2 for 24 hours followed by neurite outgrowth measurement. For CXCL13 neutralization in vivo, control IgG or CXCL13 mAb (30 mg/kg body weight) was i.p. injected into the young or aged mice 4 hours after sciatic nerve crush and daily until killing on day 3. For the chronic nerve regeneration study, 30 mg/kg body weight control IgG or CXCL13 mAb was i.p. injected three times per week until the animals were killed beginning 4 hours after injury.

Adoptive cell transfer

Spleens from wild-type or *Cxcr5*$^{-/-}$ mice were harvested. Splenocytes were extracted after red blood cell lysis using RBC lysis buffer (Biolegend, 420302). CD8$^+$ T cells were then purified with mouse CD8$^+$ T cell isolation kit (Miltenyi Biotec, 130-104-075) and LS columns (Miltenyi Biotec, 130-042-401). Wild-type CD8$^+$ T cells or *Cxcr5*$^{-/-}$ CD8$^+$ T cells (2×10^7) were i.v. injected into each aged OT-I *Rag2*$^{-/-}$ mouse (20 to 22 months old) and a sciatic nerve crush was performed 3 days after cell transfer. Control IgG or CXCL13 mAb (30 mg/kg body weight) was i.p. injected into the recipients immediately after cell transfer and daily until killing on day 3 after nerve injury. For wild-type CXCR5$^+$CD8$^+$ T cell transfer, purified CD8$^+$ T cells from spleen and lymph nodes of adult wild-type mice (4 to 6 months old) were stained with LIVE/DEAD, anti-CD8, anti-TCRβ, biotin-conjugated anti-CXCR5 antibodies for 20 min followed by washing and staining with APC-streptavidin. Live TCRβ$^+$CD8$^+$CXCR5$^+$ cells were sorted with BD FACSAria III flow cytometer. Cells (5×10^6, sorted from spleen and lymph nodes of ~10 donors) per recipient were adoptively transferred to the young (8 to 10 weeks old) and aged OT-I *Rag2*$^{-/-}$ mice (20 to 22 months old). Control groups were injected with an equivalent amount of PBS. Three days later, a sciatic nerve crush was performed, and the animals were killed 3 days after nerve injury. DRG, spleen, and blood samples were then collected after a 3-min labeling of blood-exposed cells by i.v. injection of PE-Cy7–conjugated anti-CD45. Isolated DRG cells, splenocytes, and blood cells were stained with LIVE/DEAD, primary antibodies, and tetramer (SIINFEKL) for 30 min at room temperature. The cells were washed and stained with APC-streptavidin (2 μg/ml) for 20 min at 4°C. Cell samples were acquired by flow cytometer LSR II (BD Biosciences). Detailed antibody information is provided in table S1.

In vivo administration of IKK and caspase 3 inhibitors

PS1145 (TOCRIS, #4569) was reconstituted with 0.5% methyl cellulose (Sigma), 0.2% Tween-80 (Sigma) in water. The suspension was vortexed for 2 min and sonicated at 37°C for 20 min (LabSonic, B. Braun Biotech International; 0.5-mm-diameter sonotrode, three times per 5 s, amplitude 80%). The methyl cellulose solution or PS1145 suspension was delivered at 50 mg/kg body weight by intragastric gavage immediately after sciatic nerve crush and at day 2. Specific inhibition of caspase 3 in vivo was performed by i.v. delivery of Z-DEVD-FMK (Santa Cruz, #210344-95-9) in 1% DMSO at a dosage of 20 mg/kg body weight daily after sciatic nerve injury.

Behavioral assessment

Mice with sciatic nerve crush and chronic administration (i.p. injection) of control IgG or CXCL13 mAb (30 mg/kg body weight, three times per week) were used for behavioral assessments. The left side of sciatic nerve and hindpaw were injured and behaviorally assessed at day 0 and from day 7 to day 42 followed by the tissue collection at day 43. Animals were randomly and equally grouped. All investigators participating in behavioral assessments were blind to the groups and the treatments (*41*).

Mechanical sensitivity test

Mice were placed in the test chamber for 30 min to acclimate before initiating the behavioral assessment. Mechanical sensitivity was determined by probing the plantar surface of the left hindpaw with calibrated Von Frey filaments ranging from 0.4 to 4 g. To give the sensory receptors enough time to return to baseline, the interval time was at least 30 s between each trial. A quick hindpaw withdrawal was considered a positive response. Five trials were conducted for each mouse. The withdrawal threshold to the mechanical stimulation was defined as the lowest force that resulted in at least three withdrawals in five trials, as described (*42*).

Thermal sensitivity test

For thermal sensitivity, the Hargreaves test (Ugo Basile, catalog number 37370) was performed as described (*43*, *44*). Briefly, mice were placed on a glass floor and separated by plastic chambers. Mice were given 30 min to acclimate. The thermal heat stimuli (infrared radiation source, intensity = 50) were carefully placed under the plantar surface of the hindpaw for no more than 10 s (*44*). The hindpaw withdrawal time was recorded automatically. Five trials were conducted on each paw and the average was calculated including the longest and shortest withdrawal time.

Adhesive removal

Small adhesive stimuli (6-mm round adhesive labels) were placed on the left hindpaw of the mouse. The time to make first contact with both forepaws or mouth, as well as the time to completely remove the adhesive, were then recorded. Daily 10-min training sessions per mouse were performed for 1 week prior to the nerve injury. Each mouse was subjected to three trials. All testing was performed in the

animal's home cage by a blind investigator as described (*39*, *45*).

Statistical analysis

Data were statistically analyzed with Graphpad Prism 9.3 (Graphpad Software Inc., La Jolla, CA) and expressed as mean ± SEM unless otherwise stated. Statistical comparisons were analyzed using unpaired two-tailed Student's *t* test for two groups. Multiple groups were analyzed using one-way analysis of variance (ANOVA) with post hoc Tukey's correction or two-way ANOVA with post hoc Sidak's test. Statistical significance was considered as $P < 0.05$. All experiments were replicated two or three times. The *n* defining biological replicates was always determined by power analysis with power set at 80% and significance level at 5%.

REFERENCES AND NOTES

1. M. J. DeVivo, Y. Chen, Trends in new injuries, prevalent cases, and aging with spinal cord injury. *Arch. Phys. Med. Rehabil.* **92**, 332–338 (2011). doi: 10.1016/j.apmr.2010.08.031; pmid: 21353817
2. A. Pestronk, D. B. Drachman, J. W. Griffin, Effects of aging on nerve sprouting and regeneration. *Exp. Neurol.* **70**, 65–82 (1980). doi: 10.1016/0014-4886(80)90006-0; pmid: 7418774
3. D. W. Vaughan, Effects of advancing age on peripheral nerve regeneration. *J. Comp. Neurol.* **323**, 219–237 (1992). doi: 10.1002/cne.903230207; pmid: 1401257
4. E. Verdú, D. Ceballos, J. J. Vilches, X. Navarro, Influence of aging on peripheral nerve function and regeneration. *J. Peripher. Nerv. Syst.* **5**, 191–208 (2008). doi: 10.1111/j.1529-8027.2000.00026.x; pmid: 11151980
5. H. Kang, J. W. Lichtman, Motor axon regeneration and muscle reinnervation in young adult and aged animals. *J. Neurosci.* **33**, 19480–19491 (2013). doi: 10.1523/JNEUROSCI.4067-13.2013; pmid: 24336714
6. M. W. Painter *et al*., Diminished Schwann cell repair responses underlie age-associated impaired axonal regeneration. *Neuron* **83**, 331–343 (2014). doi: 10.1016/j.neuron.2014.06.016; pmid: 25033179
7. D. Weiskopf, B. Weinberger, B. Grubeck-Loebenstein, The aging of the immune system. *Transpl. Int.* **22**, 1041–1050 (2009). doi: 10.1111/j.1432-2277.2009.00927.x; pmid: 19624493
8. N. Barzilai, D. M. Huffman, R. H. Muzumdar, A. Bartke, The critical role of metabolic pathways in aging. *Diabetes* **61**, 1315–1322 (2012). doi: 10.2337/db11-1300; pmid: 22618766
9. L. C. D. Pomatto, K. J. A. Davies, The role of declining adaptive homeostasis in ageing. *J. Physiol.* **595**, 7275–7309 (2017). doi: 10.1113/JP275072; pmid: 29028112
10. J. C. Lo *et al*., Coordination between NF-κB family members p50 and p52 is essential for mediating LTβR signals in the development and organization of secondary lymphoid tissues. *Blood* **107**, 1048–1055 (2006). doi: 10.1182/blood-2005-06-2452; pmid: 16195333
11. S. A. van de Pavert *et al*., Chemokine CXCL13 is essential for lymph node initiation and is induced by retinoic acid and neuronal stimulation. *Nat. Immunol.* **10**, 1193–1199 (2009). doi: 10.1038/ni.1789; pmid: 19783990
12. E. Dejardin *et al*., The lymphotoxin-β receptor induces different patterns of gene expression via two NF-κB pathways. *Immunity* **17**, 525–535 (2002). doi: 10.1016/S1074-7613(02)00423-5; pmid: 12387745
13. J. Levitskaya *et al*., Inhibition of antigen processing by the internal repeat region of the Epstein-Barr virus nuclear antigen-1. *Nature* **375**, 685–688 (1995). doi: 10.1038/375685a0; pmid: 7540727
14. E. R. Burnside *et al*., Immune-evasive gene switch enables regulated delivery of chondroitinase after spinal cord injury. *Brain* **141**, 2362–2381 (2018). doi: 10.1093/brain/awy158; pmid: 29912283
15. J. Chu, E. Lauretti, D. Praticò, Caspase-3-dependent cleavage of Akt modulates tau phosphorylation via GSK3β kinase: Implications for Alzheimer's disease. *Mol. Psychiatry* **22**, 1002–1008 (2017). doi: 10.1038/mp.2016.214; pmid: 28138159
16. K. Liu *et al*., PTEN deletion enhances the regenerative ability of adult corticospinal neurons. *Nat. Neurosci.* **13**, 1075–1081 (2010). doi: 10.1038/nn.2603; pmid: 20694004
17. W. Chen *et al*., Rapamycin-resistant mTOR activity is required for sensory axon regeneration induced by a conditioning lesion. *eNeuro* **3**, ENEURO.0358-16.2016 (2017). doi: 10.1523/ENEURO.0358-16.2016; pmid: 28101526
18. T. C. Jackson, A. Rani, A. Kumar, T. C. Foster, Regional hippocampal differences in AKT survival signaling across the lifespan: Implications for CA1 vulnerability with aging. *Cell Death Differ.* **16**, 439–448 (2009). doi: 10.1038/cdd.2008.171; pmid: 19039330
19. B. Du *et al*., CD4$^+$ αβ T cell infiltration into the leptomeninges of lumbar dorsal roots contributes to the transition from acute to chronic mechanical allodynia after adult rat tibial nerve injuries. *J. Neuroinflammation* **15**, 81 (2018). doi: 10.1186/s12974-018-1115-7; pmid: 29544518
20. J. G. Cyster *et al*., Follicular stromal cells and lymphocyte homing to follicles. *Immunol. Rev.* **176**, 181–193 (2003). doi: 10.1034/j.1600-065X.2000.00618.x; pmid: 11043777
21. B.-C. Jiang *et al*., CXCL13 drives spinal astrocyte activation and neuropathic pain via CXCR5. *J. Clin. Invest.* **126**, 745–761 (2016). doi: 10.1172/JCI81950; pmid: 26752644
22. X.-B. Wu *et al*., CXCL13/CXCR5 enhances sodium channel Nav1.8 current density via p38 MAP kinase in primary sensory neurons following inflammatory pain. *Sci. Rep.* **6**, 34836 (2016). doi: 10.1038/srep34836; pmid: 27708397
23. R. He *et al*., Follicular CXCR5- expressing CD8(+) T cells curtail chronic viral infection. *Nature* **537**, 412–428 (2016). doi: 10.1038/nature19317; pmid: 27501245
24. D. Yu, L. Ye, A portrait of CXCR5+ follicular cytotoxic CD8$^+$ T cells. *Trends Immunol.* **39**, 965–979 (2018). doi: 10.1016/j.it.2018.10.002; pmid: 30377045
25. B. W. Dulken *et al*., Single-cell analysis reveals T cell infiltration in old neurogenic niches. *Nature* **571**, 205–210 (2019). doi: 10.1038/s41586-019-1362-5; pmid: 31270459
26. B. Coder *et al*., Friend or foe: The dichotomous impact of T cells on neuro-de/re-generation during aging. *Oncotarget* **8**, 7116–7137 (2017). doi: 10.18632/oncotarget.12572; pmid: 27738345
27. G. Nardo *et al*., Counteracting roles of MHCI and CD8$^+$ T cells in the peripheral and central nervous system of ALS SOD1^{G93A} mice. *Mol. Neurodegener.* **13**, 42 (2018). doi: 10.1186/s13024-018-0271-7; pmid: 30092791
28. M. Daglas *et al*., Activated CD8$^+$ T Cells Cause Long-Term Neurological Impairment after Traumatic Brain Injury in Mice. *Cell Rep.* **29**, 1178–1191.e6 (2019). doi: 10.1016/j.celrep.2019.09.046; pmid: 31665632
29. A. L. Oliveira *et al*., A role for MHC class I molecules in synaptic plasticity and regeneration of neurons after axotomy. *Proc. Natl. Acad. Sci. U.S.A.* **101**, 17843–17848 (2004). doi: 10.1073/pnas.0408154101; pmid: 15591351
30. M. S. Joseph *et al*., Transgenic mice with enhanced neuronal major histocompatibility complex class I expression recover locomotor function better after spinal cord injury. *J. Neurosci. Res.* **89**, 365–372 (2011). doi: 10.1002/jnr.22557; pmid: 21259323
31. J. E. Knickelbein *et al*., Noncytotoxic lytic granule-mediated CD8$^+$ T cell inhibition of HSV-1 reactivation from neuronal latency. *Science* **322**, 268–271 (2008). doi: 10.1126/science.1164164; pmid: 18845757
32. S. G. Meuth *et al*., Cytotoxic CD8$^+$ T cell-neuron interactions: Perforin-dependent electrical silencing precedes but is not causally linked to neuronal cell death. *J. Neurosci.* **29**, 15397–15409 (2009). doi: 10.1523/JNEUROSCI.4339-09.2009; pmid: 20007464
33. M. D'Amelio, V. Cavallucci, F. Cecconi, Neuronal caspase-3 signaling: Not only cell death. *Cell Death Differ.* **17**, 1104–1114 (2010). doi: 10.1038/cdd.2009.180; pmid: 19960023
34. H. A. Wols *et al*., Migration of immature and mature B cells in the aged microenvironment. *Immunology* **129**, 278–290 (2010). doi: 10.1111/j.1365-2567.2009.03182.x; pmid: 19845796
35. J. S. Lefebvre *et al*., The aged microenvironment contributes to the age-related functional defects of CD4 T cells in mice. *Aging Cell* **11**, 732–740 (2012). doi: 10.1111/j.1474-9726.2012.00836.x; pmid: 22607653
36. E. Klimatcheva *et al*., CXCL13 antibody for the treatment of autoimmune disorders. *BMC Immunol.* **16**, 6 (2015). doi: 10.1186/s12865-015-0068-1; pmid: 25879435
37. A. R. Bauder, T. A. Ferguson, Reproducible mouse sciatic nerve crush and subsequent assessment of regeneration by whole mount muscle analysis. *J. Vis. Exp.*3606 (2012). doi: 10.3791/3606; pmid: 22395197
38. T. H. Hutson *et al*., Cbp-dependent histone acetylation mediates axon regeneration induced by environmental enrichment in rodent spinal cord injury models. *Sci. Transl. Med.* **11**, eaaw2064 (2019). doi: 10.1126/scitranslmed.aaw2064; pmid: 30971452
39. A. Hervera *et al*., Reactive oxygen species regulate axonal regeneration through the release of exosomal NADPH oxidase 2 complexes into injured axons. *Nat. Cell Biol.* **20**, 307–319 (2018). doi: 10.1038/s41556-018-0039-x; pmid: 29434374
40. Z. Keren *et al*., B-cell depletion reactivates B lymphopoiesis in the BM and rejuvenates the B lineage in aging. *Blood* **117**, 3104–3112 (2011). doi: 10.1182/blood-2010-09-307983; pmid: 21228330
41. B. Chen *et al*., Reactivation of dormant relay pathways in injured spinal cord by KCC2 manipulations. *Cell* **174**, 521–535.e13 (2018). doi: 10.1016/j.cell.2018.06.005; pmid: 30033363
42. S. J. Gladman *et al*., Improved outcome after peripheral nerve injury in mice with increased levels of endogenous ω-3 polyunsaturated fatty acids. *J. Neurosci.* **32**, 563–571 (2012). doi: 10.1523/JNEUROSCI.3371-11.2012; pmid: 22238091
43. A. C. Ogbonna, A. K. Clark, M. Malcangio, Development of monosodium acetate-induced osteoarthritis and inflammatory pain in ageing mice. *Age* **37**, 54 (2015). doi: 10.1007/s11357-015-9792-y; pmid: 25971876
44. N. Agarwal *et al*., Evoked hypoalgesia is accompanied by tonic pain and immune cell infiltration in the dorsal root ganglia at late stages of diabetic neuropathy in mice. *Mol. Pain* **14**, 1744806918817975 (2018). doi: 10.1177/1744806918817975; pmid: 30453826
45. S. M. Fleming *et al*., Early and progressive sensorimotor anomalies in mice overexpressing wild-type human α-synuclein. *J. Neurosci.* **24**, 9434–9440 (2004). doi: 10.1523/JNEUROSCI.3080-04.2004; pmid: 15496679

ACKNOWLEDGMENTS

We thank M. Jucker for providing several aged wild-type mice, M. Merkenschlager and J. Fawcett for their critical feedback on the manuscript, T. Arnon and her team for providing material from *Cxcr5*$^{-/-}$ mice, the LMS/NIHR Imperial Biomedical Research Center Flow Cytometry Facility for support, and N. Haberman for advice on statistical analysis. **Funding:** Supported by Wings for Life, The Rosetrees Trust, the National Institute for Health Research (NIHR) Imperial Biomedical Research Centre, Guarantors of Brain (L.Z.), and start-up funds from the Department of Brain Sciences, BRC funds, Imperial College London (S.D.G.) and Wings for Life grant WFL-NL-25/20 (J.V.). The views expressed are those of the author(s) and not necessarily those of the NHS, the NIHR, or the UK Department of Health. **Author contributions:** L.Z. designed and performed experiments and data analysis and wrote the paper; G.K. designed and performed experiments and performed data analysis; I.P. designed experiments and performed data analysis; M.D. performed data analysis; G.C. performed experiments; F.D.V. performed experiments; M.T.C. performed data analysis; J.S.C. performed experiments; Z.Y. performed experiments; V.L. provided experimental advice and edited the paper; J.B. provided experimental advice; R.P. provided experimental advice and edited the paper; J.V. provided research material for experiments and edited the paper; F.D.W. provided research material for experiments; C.P. provided research material for experiments and experimental advice; C.L.C. provided research material and experimental advice; J.S. provided experimental advice and edited the paper; M.B. provided experimental advice and edited the paper; S.D.G. designed experiments, provided funding, and wrote the paper. **Competing interests:** L.Z. and S.D.G. have a pending patent application related to this work titled "Use of CXCL13 Binding Molecules to Promote Peripheral Nerve Regeneration." The authors declare that they have no other competing interests. **Data and materials availability:** The raw RNA-seq data used and generated in this study have been deposited in the GEO database under accession numbers GSE138769 and GSE149770. All other data are available in the main text or supplementary materials.

SUPPLEMENTARY MATERIALS

science.org/doi/10.1126/science.abd5926
Figs. S1 to S19
Table S1
Data S1 to S3

Submitted 3 July 2020; resubmitted 22 September 2021
Accepted 9 March 2022
10.1126/science.abd5926